Image and Vision Computing 29 (2011) 509–523

Contents lists available at ScienceDirect

Image and Vision Computing

journal homepage: www.elsevier.com/locate/imavis

Review article

A survey on image-based continuum-body motion estimation ☆

Wei Liu, Eraldo Ribeiro *

Computer Vision and Bio-Inspired Computing Laboratory, Department of Computer Sciences, Florida Institute of Technology, Melbourne, FL 32901, USA

ARTICLE INFO

Article history:
Received 8 July 2010
Received in revised form 31 January 2011
Accepted 22 March 2011

Keywords:
Nonrigid image registration
Continuum motion
Meshless registration methods

ABSTRACT

This paper presents a survey of the state-of-the-art in motion estimation of continuum objects such as elastic solids (e.g., human organs, skin, and biomedical tissues) and fluids (e.g., clouds, ocean flows, and air flows). The survey is focused on the estimation methodologies, rather than on specific applications. We begin by summarizing the main components and challenges of continuum-motion estimation, and structure our review around these components. We provide a classification of the related work according to their solutions to these challenges. A discussion on the methodologies for quantitative evaluation of methods is also provided. Finally, we conclude the survey by pointing out some open problems in continuum-motion estimation.

Contents

☆ This paper has been recommended for acceptance by Cornelia M Fermuller.

* Corresponding author. Tel.: +1 321 674 8149.
E-mail address: eribeiro@cs.fit.edu (E. Ribeiro).

0262-8856/$ – see front matter © 2011 Elsevier B.V. All rights reserved.
doi:10.1016/j.imavis.2011.03.003

1. Introduction

Motion estimation is a key task in computer vision, and it is usually the first step taken towards understanding and analyzing dynamic visual phenomena. Generally, the goal of motion estimation is to recover a dense displacement field from a pair or a sequence of images. For example, one of the most extensively studied motion-estimation problems is that of recovering an individual pixel's apparent motion, i.e., the optical flow field [1]. The motion estimation problem can also present itself in different forms such as image registration [2], where a template object is aligned and sometimes warped to a target image. In image registration terminology, the displacement field is called a *deformation field* or *warping function*.

Depending on their complexity, motion patterns can be divided into simpler linear (affine) and more complicated nonlinear motions [4]. On one hand, motions that can be represented by an affine transformation are parameterized by a six-parameter linear model (i.e., scaling, rotation, and translation) that can be used to describe projected 2-D motions originated from processes such as camera zooming, rotation, and panning as well as from the relative motion of a rigid object. On the other hand, nonlinear motions usually result from the deformation of nonrigid objects, involving complicated physical processes, such as articulated human motion [5], fluid motion [6], and biomechanical deformation [7]. Among nonlinear motions, articulated human motion is worthy of a separate survey [8]. In this survey, we focus ourselves on the problem of estimating motions resulting from continuum mechanics, i.e., nonrigid deformations of elastic objects, such as fluid motion and biomedical motions. Fig. 1 shows examples and a hierarchical relationship of different types of motion. Motion of continuum objects is ubiquitous in many different applications, but their estimation methods share basic common principles. For example, the spline-based model commonly used in medical image registration was recently extended for fluid-motion estimation [9]. On the other hand, viscous fluid models have been extensively used in image registration [10]. Given the relevance of continuum-motion estimation, instead of limiting the discussion to a single application domain, we decided that this survey will present an overview of different applications, and a classification of existing approaches according to their common components. More specifically, we focus our survey on the following applications:

- Biomedical image analysis. The goal of medical image registration [2,11] is to recover deformation fields from MRI, CT, or X-ray images of human organs undergoing nonrigid deformations due to physiological processes or inter-subject variations. Applications of registration include motion compensation [2], diagnosis [12,13], and segmentation [14]. Besides registration, the analysis of soft tissues such as human faces [15] and skin [16] also requires estimating their nonrigid continuous deformations.
- Fluid motion analysis. Fluid motion estimation has enjoyed renewed attention recently, in both engineering and science applications. For example, estimating fluid motion from particle image velocimetry (PIV) images is important for understanding and verifying mechanical models [3,17,18]. It can also help analyze turbulent ocean currents [19], recover cloud motion from satellite images [20], and detect cyclones [21]. Finally, fluid motion also exists in biomedical applications such as blood flow [22,23], and viscous cell motion [7].

There are a number of surveys on medical image registration [2,11,24]. However, these surveys tend to focus on applications rather than technologies, and none of them provide a comprehensive review of the physics and parametric models underlying the approaches. An exception to this trend is a recent survey by Holden [25] that reviewed the physics and geometric models used in nonrigid registration. Our survey is similar to [25], but we extend our target objects to include fluids, and discuss recently developed *meshless methods*. On one hand, fluids are continuum objects, and fluid motion estimation is intrinsically related to nonrigid image registration. Additionally, fluid models have been extensively used in medical image registration. By including fluids into discussion, our survey provides a broad and complete view of the analysis and estimation of continuum objects. On the other hand, there is a recent trend to relax the geometric and physics models used for handling large deformations, or to adapting the registration to object shape and image content. This direction is taken by the so-called meshless methods, and contrasts with the way classic parametric

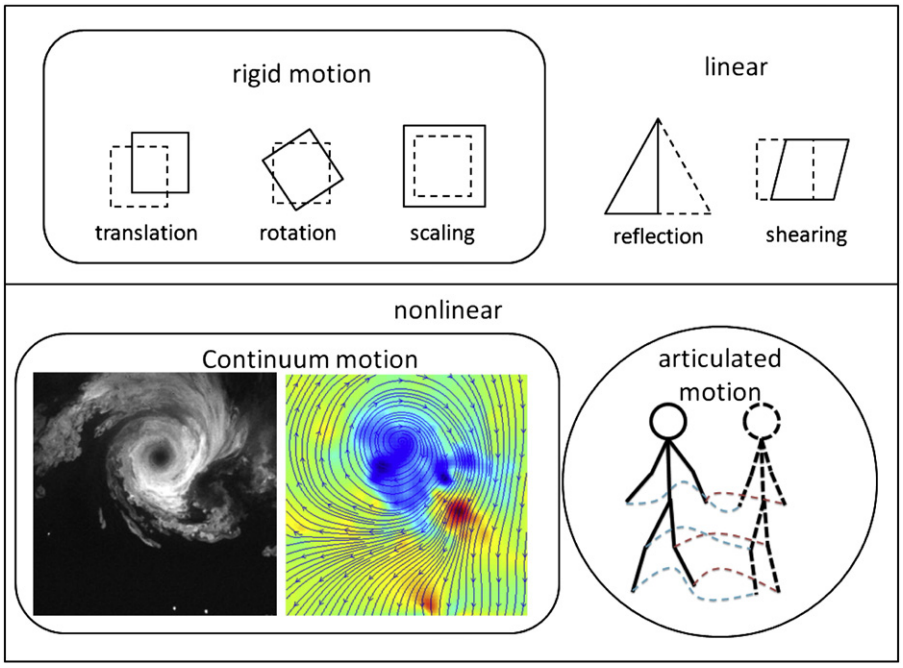

Fig. 1. The relationship of different types of motion. Motion models can be divided into linear and nonlinear. Linear motions include rigid motion (translation, rotation, and scaling), plus reflection and shearing, while nonlinear motions include continuum (e.g., fluid flow [3] and elastic solid deformation) and articulated motions.

models partition the computation domain, and represents a global deformation field by assembling local deformation fields based on their neighboring information. In classic approaches, the partition and neighborhood information are often explicitly handled using a grid (mesh) of control points [25]. Compared to these methods, meshless models do not rely on control-point grids, and they are able to handle objects of arbitrary shape and topologies. Meshless methods have already been used in a large number of applications [26–29], and we found appropriate to include these works in the survey.

Our main goal is to provide an overview of both the modeling and estimation methods for continuum body motion analysis. To archive this goal, we commence by providing a general formulation of the nonrigid motion estimation problem as well of its main components and challenges (Section 2). We then discuss the various representative approaches for these components and challenges of the nonrigid motion estimation problem. First, we discuss the image similarity measures used to establish correspondence between pixels of the deformed images (Section 3). A deformation field can be defined as the one that maximizes the similarity between the source and the deformed target images. As images are subject to noise and illuminance changes, similarity measures need to be robust. Additionally, there are also similarity measures defined on images of different modalities. Secondly, we discuss parametric deformation models in Section 4. These models significantly improve motion estimation for continuum objects, by producing smooth results while reducing the solution space's dimensionality. In this section, we classify and introduce classic deformation models, and explain recently proposed meshless models. After reviewing the parametric models, we discuss the physics laws and smoothness heuristics that can be used to address the inherent ill-posedness of the motion-estimation problem by regularizing the deformation field to produce physically or geometrically meaningful results (Section 5). In Section 6, we provide a discussion of the methodologies for quantitative evaluation of continuum-body motion-estimation methods. Finally, we conclude the survey in Section 7, and present a number of future directions that we believe are promising. In particular, we believe that meshless methods may allow us to naturally integrate computer graphics and physics models with image evidence, and improve motion estimation and analysis in many challenging applications including facial expressions, fluid motion, and other 3-D nonrigid continuum motions.

2. Problem formulation and challenges

The problem of nonrigid motion estimation can be formulated as that of finding a transformation that warps source image $I(\mathbf{x})$ to "best" match target image $I'(\mathbf{x})$ with respect to a given similarity measure [29]. Formally, we seek for a warping or deformation field $\mathbf{u}(\mathbf{x})$ that satisfies the following equation:

$$\arg\max_{\mathbf{x}'} F(I'(\mathbf{x}'), I(\mathbf{x})), \quad \mathbf{x}' = \mathbf{x} + \mathbf{u}(\mathbf{x}), \tag{1}$$

where $\mathbf{x}$ is a coordinate vector, $\mathbf{x}'$ is the warping function that indicates the transformed coordinates. $\mathbf{x}'$ can also be expressed as the deformation (displacement) field $\mathbf{u}(\mathbf{x})$, and F is a similarity measure. Fig. 2 shows an example illustrating a nonrigid image registration and corresponding deformation fields.

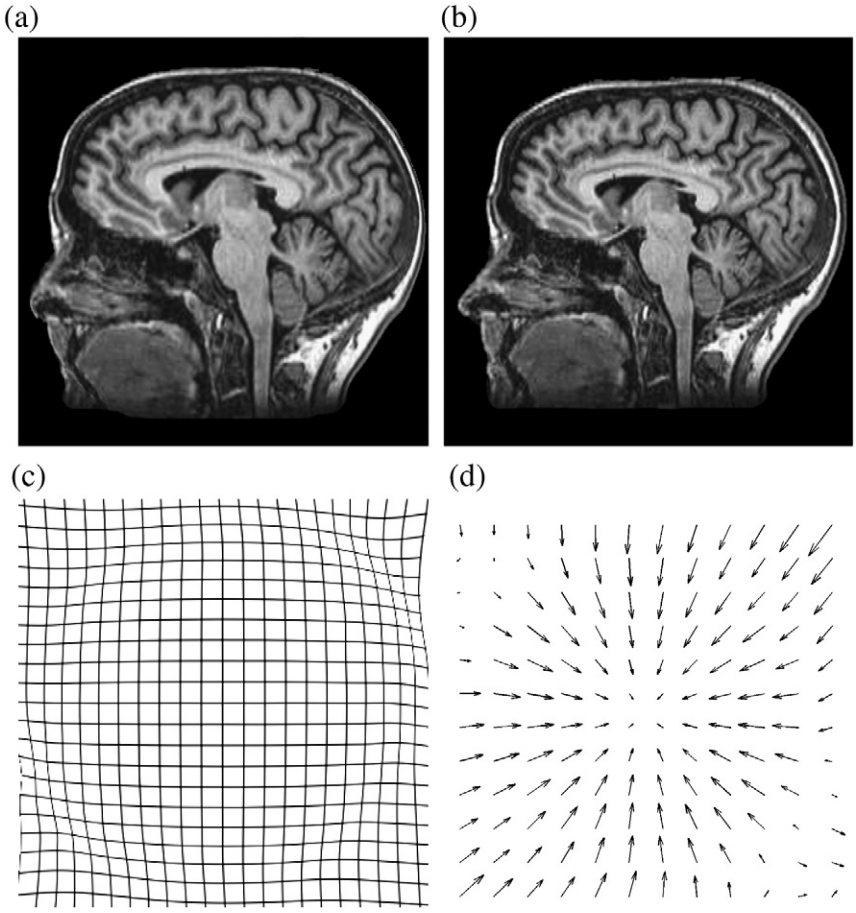

Fig. 2. Nonrigid image registration. (a) Source image. (b) Target image. (c) Deformation field as a distorted grid. (d) Deformation field as a vector field.

Despite its simplicity, there are major challenges in solving the motion-estimation equation in Eq. (1). These challenges are:

- The designing of the similarity measure. In the simplest case, the image similarity can be measured by the squared-difference between pixel intensities of the corresponding source and target images, i.e., $F(I'(\mathbf{x}'), I(\mathbf{x}), \mathbf{x}') = \sum_{\mathbf{x}} \|I'(\mathbf{x}') - I(\mathbf{x})\|^2$. This measure relies on the assumption that image intensities remain constant during the motion, and can be equivalently discretized into the widely used optical-flow constraint [1]:

$$\frac{\partial I}{\partial t} + \mathbf{u} \cdot \nabla I = 0 \tag{2}$$

  Eq. (2) states that the temporal variation in the image, $\frac{\partial I}{\partial t}$, cancels the projection of local displacement vector $\mathbf{u}$ on the image gradient vector ∇I. However, the intensity-constancy assumption does not always hold for large continuum motions. For example, the dilution or concentration of continuum mass may decrease or increase image intensities [6], and thus render the intensity-constancy constraint invalid. Image noise and variation in illumination can also violate this assumption [30]. Thus, robust similarity measures are needed for handling outliers. Additionally, when source and target images are obtained using different imaging sensors (multi-modality), as in the case of MRI and CT images, then image intensities cannot be compared directly, and sophisticated similarity measures are required [31].
- Modeling the deformation field. Unlike optical flow computation, where the deformation field $\mathbf{u}$ is usually unstructured, the motion of continuum objects often results from "well-behaved" physics processes. As a result, this kind of motion is often represented using parametric models such as polynomials [25]. The use of parametric models not only increase robustness of registration algorithms against random noise, but also provides a compact representation of the deformation field, leading to improved computational efficiency in motion estimation.
- Integrating prior information. The physics and biological-based nature of continuum motions allows for prior information of materials to be integrated to improve temporal consistency of the motion estimation, as well as to further regulate solutions. Many existing algorithms for solving physics equations have been extended and adapted to solve the motion estimation problem [25].
- Regulating the solutions. In the absence of accurate physics or statistical prior models, the motion estimation equation in Eq. (1) has many ambiguous solutions, and regularizers are needed to produce unique estimation results. On one hand, the main goals of a regularizer are to penalize undesired distortion, and produce "smooth" deformation fields. On the other hand, regularizers should also be flexible, and not rule out legitimate solutions.

3. Measuring image similarity

The function F in Eq. (1) measures the similarity of local image data, providing evidence to guide the motion estimation process. As mentioned previously, the commonly used squared-difference of image intensities might not hold for large deformations, and is not appropriate if the images are obtained using different image sensors (i.e., multi-modal data). The multi-modality problem is typical in medical image registration. To address these shortcomings, a number of similarity measures have been recently proposed. Next, we describe a few representative similarity measures.

3.1. Inter-modality similarity

The challenge of measuring similarity between images of different modalities lies in the fact that obtaining an exact relationship between the modalities can be prohibitively complicated. Inter-modality similarity is not our focus in this survey, but we describe it here for completeness. One of the most commonly used similarity measure for images of different modalities is based on mutual information (MI) [32,33]. This is a statistical measure that quantifies the dependence between two random variables and it is based on the assumption that, when two images of different modalities are correctly matched, one image should be predictable from the other image. This predictability can be measured using the mutual information between their intensity or image feature distributions. Given its statistical nature, the calculation of mutual information does not rely on an exact relationship between different modalities, and thus greatly simplifies the similarity measure in image registration. For more details on the application of the MI similarity measure, please refer to [31].

3.2. Dilution and concentration

For images of the same modality, a frequently used similarity measure is based on the assumption that image intensity values remain constant during continuum motion. However, when the deformation field is large, dilution and concentration of the continuum mass will change local densities, making the brightness-constancy assumption invalid. Dilution and concentration effects can be addressed by modeling density variations of the moving continuum material using the following continuity equation [6]:

$$\frac{\partial \rho}{\partial t} + \operatorname{div}(\rho \mathbf{u}) = \frac{\partial \rho}{\partial \mathrm{t}} + \nabla \rho \cdot \mathbf{u} + \rho \operatorname{div}(\mathbf{u}) = 0, \tag{3}$$

where ρ is the mass density, and $\mathbf{u}$ is the deformation field. Whenever the image intensity is proportional to mass intensity, Eq. (3) can be used to replace the optical-flow equation in Eq. (2). Alternatively, it can be shown that the image intensities are proportional to the integral of mass density. In this case, the relationship between the source and target images can be expressed by [6]:

$$I'(\mathbf{x}') = I(\mathbf{x}) \exp(-\operatorname{div} \mathbf{u}). \tag{4}$$

Eq. (4) is called the mass-constancy constraint as it assumes that the mass within a deforming boundary remains constant, and it is equivalent to the classical brightness-constancy for divergence-free deformations, i.e., $\operatorname{div} \mathbf{u} = 0$. This constraint has been widely used in both fluid-motion estimation [9,19,34], and in medical image registration [35–37].

3.3. Robust similarity measures

Similarity measures based on squared-difference can be sensitive to illumination changes and to the presence of noise. For example, the presence of sensor-induced additive Gaussian noise is common in many applications. This noise modality is modeled by many motion-estimation approaches as a stationary distribution that does not vary with spatial coordinates [24,38]. Besides stationary Gaussian noise, real-world imagery may contain spatially varying distortions, occlusions, and specular-reflectance artifacts [39]. For instance, in medical imaging, the data may contain an intensity bias varying slowly and spatially [40] across the image. Specular reflection is yet another source of unwanted artifacts that tend to appear in images of biological tissues such as human skin [41], bones [42], and blood vessels [43]. In fluid particle image velocimetry (PIV) images, particles can be occluded [44], and handling these occlusions is key to improving motion-estimation accuracy [17].

Robustness of similarity measures can be obtained in a number of ways. First, instead of relying on individual pixel values, higher-level and neighborhood information can be included into the similarity measure. For example, a simple extension of the squared-difference

similarity is to sum it up around neighborhoods centered at the pixel being compared as follows:

$$F(\mathbf{x}) = \sum_{\mathbf{x}\in N(\mathbf{x})} \left[I(\mathbf{x}) - I'(\mathbf{x}+\mathbf{u})\right]^2, \tag{5}$$

where $N(\mathbf{x})$ is the neighborhood centered at $\mathbf{x}$. The sum-of-squared-difference (SSD) can be more robust than the difference calculated on individual pixels if image noise is stationary. However, SSD can still be sensitive to global illumination variations. In this case, the normalized cross-correlation (NCC) provides a similarity measurement that is largely independent of global illumination. Formally, NCC is defined as:

$$F(\mathbf{x}) = \frac{\sum_{\mathbf{x}\in N(\mathbf{x})}\left[I(\mathbf{x}) \times I'(\mathbf{x}+\mathbf{u})\right]}{\left[\sum_{\mathbf{x}\in N(\mathbf{x})} I^2(\mathbf{x})\right]\left[\sum_{\mathbf{x}\in N(\mathbf{x})} I'^2(\mathbf{x}+\mathbf{u})\right]}. \tag{6}$$

SSD and NCC are widely used both in image registration [2] and in fluid-motion estimation [17]. Both measures are purely intensity-based, low-level, image-similarity measures. Robustness can be further increased based on higher-level information. For example, Shen et al. [45] calculate image moments from cubic neighborhoods of individual pixels, and then the similarity is defined on the moments instead of image intensities. Image moments are integral transforms of image intensity using polynomial kernel functions, and are defined as:

$$M_{p,q} = \int\int_{\Omega} I(x,y) x^p y^q dxdy, \tag{7}$$

where Ω is the image's support domain, and $M_{p,q}$ is called the image moment of order (p,q). Since image moments are integral transformations of local intensity values, they are known to be robust to image noise. Image similarities can also be compared using other integral transforms such as Fourier-based cross-correlation [46], and phase-only correlation [47].

In addition to integral transformations, geometrical image features can also be used as similarity measures. For example, image gradients are insensitive to global illumination variation. In their work on optical-flow estimation, Brox et al. [30] considered both squared-distance of image intensities and gradients to be part of a similarity measure:

$$F(I'(\mathbf{x}'), I(\mathbf{x}), \mathbf{x}') = \sum_{\mathbf{x}} \left(\|I'(\mathbf{x}') - I(\mathbf{x})\|^2 + \lambda\|\nabla I'(\mathbf{x}') - \nabla I(\mathbf{x})\|^2\right). \tag{8}$$

From the image intensities and image gradients, a number of useful feature descriptors can be extracted (e.g., image edges, corners, and histograms), and integrated into the similarity measure. These higher-level features tend to be invariant under illumination variation, and contain more semantic information. More details of different features used in medical-image registration can be found in [2,11].

Finally, existing similarity measures can be augmented with robust estimators that use statistical priors to reduce the influence of outliers. For example, a robust version of the correlation-based similarity measure was extended by Kim and Fessler [48]. Robust estimators were used to handle outliers in image gradients [49] and, in combination with color-based similarity measures, to estimate facial motion under occlusions as described by Pantic and Patras [41]. In fluid-flow estimation, robust estimators were shown to be key in achieving high accuracy on real-world imagery [17,44]. In optical-flow estimation, a significant amount of work was devoted to the handling of outliers at motion boundaries [50–52]. These outliers are usually caused not by image-intensity variations, but by discontinuities in the deformation field. Nevertheless, the adoption of robust estimators in this case is similar to the handling of intensity outliers.

4. Parametric deformation representation

As we mentioned earlier, the motion estimation problem is ill-posed in the sense that there are many local minima in the registration equation (Eq. (1)). The ill-posedness and noise sensitivity are usually addressed by a combination of techniques, including the use of regularizers, prior information, and parametric modeling of the deformation field. In this section, we begin by discussing parametric models for continuum motions, i.e., models representing the warping function $\mathbf{x}'$, or equivalently, the deformation field $\mathbf{u} = (u,v)^T$ (Eq. (1)). In optical flow estimation, the use of parametric models often leads to only marginal improvements in estimation results [53]. However, for continuum motions, parametric models significantly increase the robustness and accuracy of results, as they often capture the inherent continuity of the underlying physics processes. In Table 1, we list common parametric models and their representative works. As shown in the table, parametric deformation models can be divided into *linear* and *nonlinear*.

Linear models represent deformation fields $\mathbf{u} = (u,v)^T$ using linear functions (Section 4.1), while nonlinear models usually use polynomials [54], radial basis function (RBF) [29,55], and polynomial splines [56,57] to represent more complicated motions (Section 4.2). Linear models are both simple and computationally efficient, but are restricted to linear transformations. On the other hand, nonlinear models offer more flexibility at higher computational costs. Deformation models can be also grouped into *local* or *global*, depending on whether they use locally or globally supported basis functions to model image deformation [2,25]. Here, the term locally supported refers to the basis functions vanishing quickly with increasing distance to their coordinate centers (e.g., the radial basis function $e^{-(x^2+y^2)}$), in which each basis function models part of the image, forming a partition of the image domain. The term globally supported means that basis functions take non-zero value over the whole image domain and model the entire image deformation. Finally, existing local models often rely on the subdivision of the computational domain, usually with the use of a regular control-point grid [29,56,57]. This greatly restricts their ability to handle irregular shapes and topological challenges. There is an important class of recently proposed nonlinear local models that do not rely on the use of control-point grids, and they form the basis of the so-called meshless (or mesh-free methods) in mechanical engineering [58]. In this survey, we briefly introduce some meshless models and their applications in computer graphics, computer vision, and engineering (Section 4.3).

It is worth pointing out that parametric modeling of continuous functions is also used in many other applications, such as representing geometric shapes (e.g., surfaces and curves) in computer graphics [59], and approximating physics variables (e.g., heat, mechanical energy, and stress) in mechanical engineering [58]. These modeling problems are intrinsically equivalent to modeling deformation fields. Additionally, parametric models for approximation and interpolation have been extensively studied in computational mathematics [55,60]. As a result, our discussion of parametric models may sometimes go beyond the modeling of deformation fields.

Table 1
Parametric deformation models.

Model		Representative works
Linear	Rigid	[61]
	Affine	[62–65]
Nonlinear	Polynomials	[66,67]
	Thin-plate splines (TPS)	[29,68,69]
	B-splines	[56]
	Finite elements (meshes)	[70–73]
	Mesh-free	[26,28,74,75]

4.1. Linear models

Rigid and affine transformations are typical linear approaches used to represent global image deformations. Rigid global motions include rotation, scaling, and shifting, and can be formally expressed as a linear transformation:

$$\mathbf{x}' = s\mathbf{R}\mathbf{x} + \mathbf{T}, \tag{9}$$

where $s \in \mathbb{R}$ is the scaling factor, $\mathbf{T} \in \mathbb{R}^n$ is the translation vector (i.e., shift), and $\mathbf{R} \in \mathbf{SL}(n)$[1] is the rotation matrix.

Rigid transformations are simple, but are also restricted to nonrigid continuum motions. The rigid motion model can be extended into a general linear transformation (i.e., affine model), or formally $\mathbf{x}' = \mathbf{A}\mathbf{x} + \mathbf{T}$, where $\mathbf{A} \in \mathbf{GL}(n)$.[2] For example, 2-D affine models extend the rigid motion model by relaxing it into the following six-parameter linear model:

$$x' = ax + by + c \text{ and } y' = dx + ey + f. \tag{10}$$

In addition to rigid transformations (scaling, rotation, and translation), an affine model can represent reflection, anisotropic scaling, and shearing effects. Global affine models are not able to model continuum motions properly, as these deformations are generally nonlinear.

4.2. Nonlinear motion models

Linear models are generally used to represent global rigid deformations of a continuum-body such as rotation and shifting, but are unable to represent nonrigid local deformations such as elastic deformation and fluid motion. To represent nonrigid local deformations, researchers resort to nonlinear or piecewise-linear models.

4.2.1. Polynomials

Polynomial models offer a straightforward extension to linear models. For example, in the 2-D case, the local deformation field in x and y can be written as [54]:

$$x' = \sum_{s,t=0} x^s y^t \text{ and } y' = \sum_{s,t=0} x^s y^t. \tag{11}$$

Indeed, polynomial models have been used for optical-flow computation [53], articulated motion [66], fluid-motion estimation [67], and image registration [54,76]. Polynomials are significantly more flexible than linear models. However, polynomials do not have local support, and their values grow exponentially with the distance to the origin. Thus, the shape of a higher-order polynomial can be sensitive to the value of its coefficients, leading to numerical instability. As a result, higher-order polynomials are often modified into local models, and their support is restricted by means of cut-off functions [77] or radial-basis functions [29].

4.2.2. Free-from deformation (FFD)

In contrast with polynomials, splines are much easier to control, and their basis functions are locally supported. Typical spline models used for image registration are based on B-splines [56,79]. B-splines use regularly distributed control points that do not need to be landmarks (i.e., features of interest on the images). B-splines are widely used in computer graphics for modeling curves or surfaces [80], and can be highly flexible in modeling nonlinear nonrigid continuum motion, e.g., biological tissues [56] or even turbulent flows [19]. In 3-D space, a cubic interpolation function is expressed as [56]:

$$\mathbf{u}(x) = \sum_{l=0}^{3}\sum_{m=0}^{3}\sum_{n=0}^{3} B_l(u)B_m(v)B_n(w)\phi_{i+l,j+m,k+n}, \tag{12}$$

where i, j, and k are the indices of neighboring control points, u, v, and w are the local coordinates, and B_i, $i = 0, 1, 2, 3$ are the spline functions. Fig. 3 shows an example of the control points, and the deformation in 3-D for a simple tubular structure. Despite the popularity of spline-based models, the reliance on a regular grid of control points restricts their adaptability. For example, the use of denser control-point grids increases accuracy at higher computational cost, and it is difficult to change control points' topology.

Recently, the B-spline model was extended to a multivariate spline model [57], a technique that greatly relaxes the positioning of control points (Fig. 4) by using simplex splines (Fig. 5), and an irregular placement of control points. However, as in most spline-based and piecewise-linear models, explicit neighborhood information is still needed.

Interestingly, these methods' reliance on a control-point grid (or mesh) is also shared in computer graphics, and mechanical engineering. For example, in computer graphics, triangular meshes are extensively used for both shape modeling and rendering, but most algorithms working on triangular meshes require topologically consistent two-manifold surfaces [81,82] (i.e., the surfaces do not 'break' or 'merge' during the motion), and dynamically adapting the resolution and topology of triangular meshes can be difficult [83,84]. In mechanical engineering, piecewise-linear models and splines are used in finite-element methods to approximate continuous functions. These methods are also restricted in both their approximation accuracy and topology adaptation.

4.2.3. Finite-element (mesh) models (FEM)

In this section, we briefly review the mesh models used in computer graphics and FEM. In computer graphics, triangular meshes are powerful tools for modeling shapes and surfaces [86], as they can be designed to represent both arbitrary topology and surface curvatures. However, dynamically adapting topology requires complicated re-meshing techniques. As piecewise-linear models, triangular meshes only ensure C^1 continuity, and the approximation accuracy depends on the triangular density (Fig. 6(a)).

Similar approximation methodology is used in finite-element methods [16,72,73] for solving partial differential equations. FEMs also rely on a mesh of explicitly connected elements. Again, maintaining the neighborhood information is nontrivial, and designing a mesh for representing complicated shapes may require intensive manual

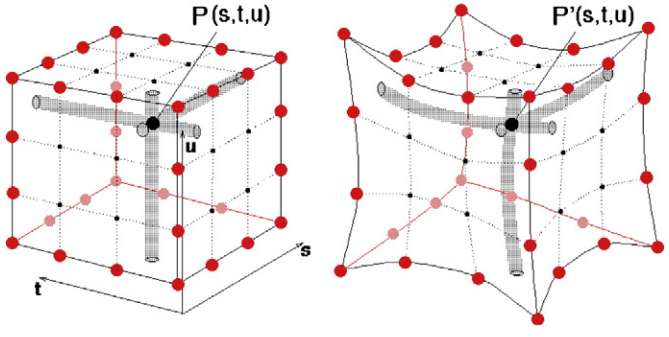

Fig. 3. Example of free-form deformation using B-splines [78]. The deformation field is controlled by a grid of control-points (the red and black dots) distributed regularly in the 3-D space with coordinates (s, t, u). Motion at control points is interpolated smoothly over the image domain. $\mathbf{P}(s, t, u)$ and $\mathbf{P}'(s, t, u)$ indicate the coordinates of point $\mathbf{P}$ before and after deformation.

[1] $SL(n)$ means *special linear group*, i.e., n-dimensional square matrices with unit determinant.

[2] $GL(n)$ means *general linear group*, i.e., n-dimensional invertible square matrices.

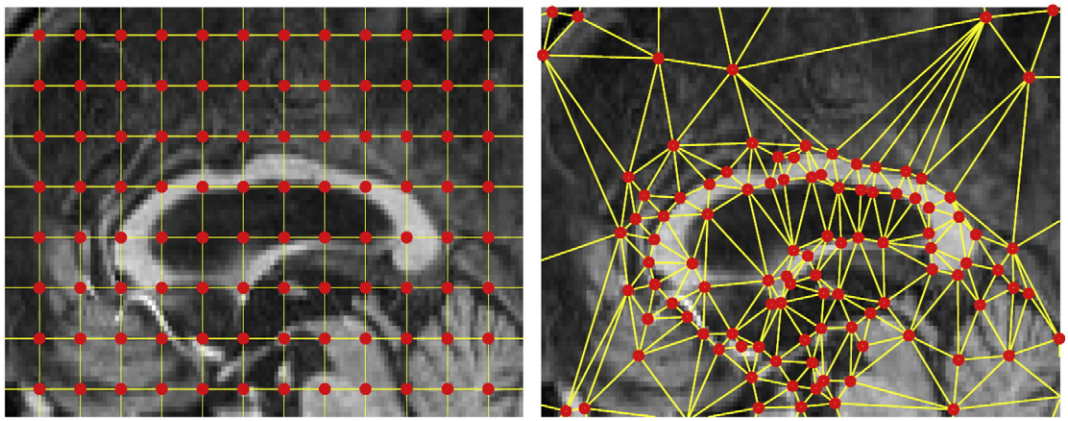

Fig. 4. Control points for B-spline and multivariate spline models [57]. The left-hand side shows a regular control-point grid for the B-spline model, and the right-hand side shows the control points for simplex splines.

interaction. For example, Fig. 6(b) shows a 3-D heart shape modeled using a mesh of 3-D volume elements, where the stress distribution is represented by a piecewise-linear function defined on the heart volume [86].

FEMs are widely used in physical science, mechanic engineering, computer graphics [87] for continuum-motion simulation, and they also have been used in computer vision for solving inverse problems. For example, FEM meshes were used for modeling 3-D nonrigid facial motion [15], and for validating motion estimation results of human tissue [71]. Triangular meshes, spline models, and FEM meshes share a similar limitation: the approximation function directly relies on the spatial arrangement of the control points. In order to remove the model's reliance on control points or elements, this scheme was recently replaced with more flexible schemes that do not rely on a control-point grid or a mesh of elements for representing continuous functions, and are collectively called mesh-free or meshless methods [28,58]. For example, in point-based computer graphics [59,88], triangular geometric primitives are replaced by sample points, and point-based representations that allow for more flexibility without the need to both store and maintain globally consistent connectivity information [59]. In Table 2, we list the applications of meshless models and corresponding representative works. There are numerous meshless models and variants in different application areas. In this survey, we focus on three representative models: radial basis functions (RBFs), weighted least-squares (WLS) with partition-of-unity, and moving least-squares (MLS).

4.3. Meshless models

4.3.1. Radial basis functions and thin-plate splines

The limitation of piecewise-linear or polynomial models was also observed in computational mathematics for both approximating and interpolating scattered data points [55,60]. As Buhmann pointed out in [55], splines or piecewise-polynomial methods usually require triangulation of the computational domain as it has to be decided where the pieces of the piecewise polynomials lie, and where they are joined together. Radial basis functions, on the other hand, can be placed at arbitrary sites in the computational domain, and a continuous function can be approximated by their linear combination. Radial basis functions (RBF) have been widely used in computer vision to represent both 2-D

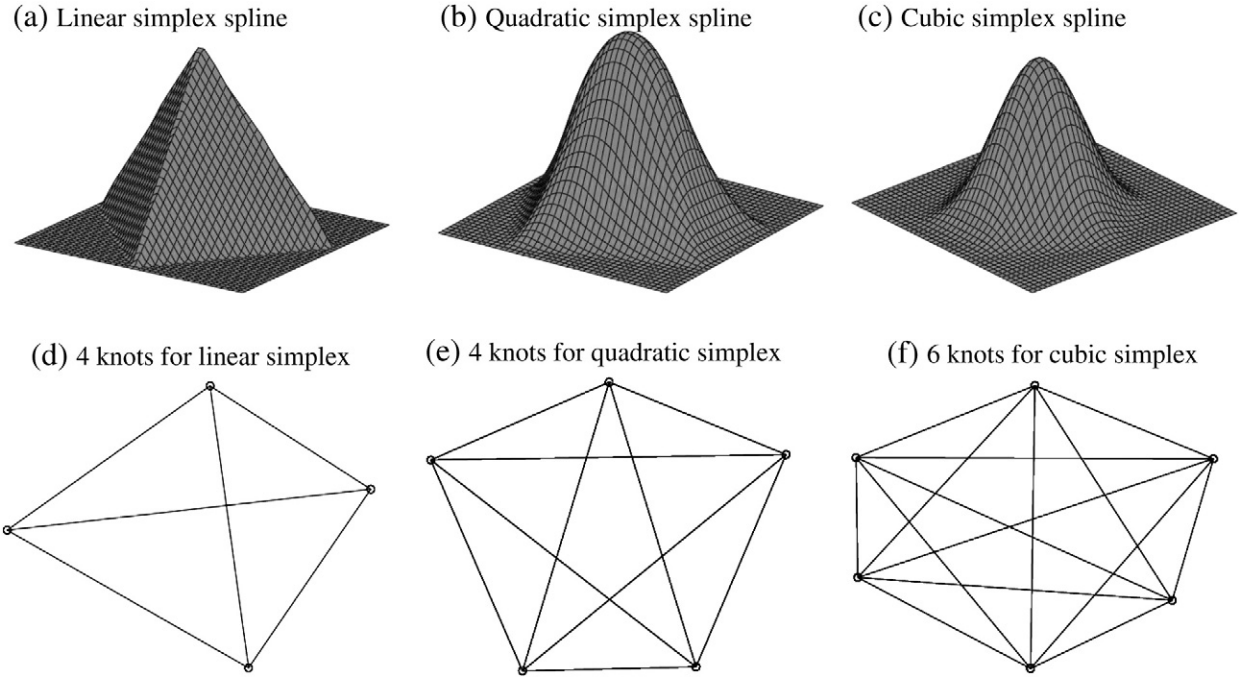

Fig. 5. Simplex splines of different degrees [57].

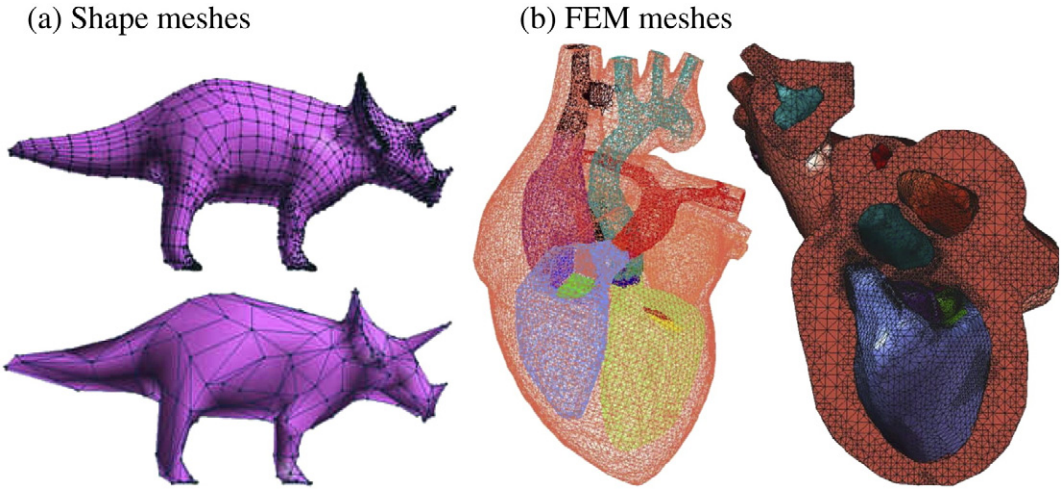

Fig. 6. Meshes in computer graphics and finite-element methods. (a) Quadrangular and triangular meshes used for shape representation in computer graphics. Denser meshes produce more details at higher computational cost [85]. (b) Shape functions constructed in finite-element methods. Anatomical parts of a heart are modeled separately using triangular meshes, then physical properties (e.g., stress and strain) are approximated as piecewise polynomial functions [86].

or 3-D nonrigid deformations [29,68,93]. Fig. 7 shows the general idea and applications of RBFs-based models. Formally, a deformation field is represented using a linear combination of radial basis functions centered at a set of points w_i with spatial coordinates $\mathbf{w}_i$:

$$\mathbf{u}(\mathbf{x}) = \sum_{k=1}^{K} c_i \phi(\|\mathbf{x}-\mathbf{w}_i\|). \tag{13}$$

Here, $\{c_i\}$ are the combination coefficients, and the radial basis functions $\phi(r)$ can be defined as a Gaussian function $\phi(r)=e^{-r^2/\sigma^2}$ or $\phi(r)=r^2 \log r$. The deformation field in Eq. (13) is often regulated by a functional similar to a thin-plate's bending energy, and it is sometimes called thin-plate splines (TPS). Thin-plate splines are normally used in conjunction with higher-level image similarity functions, where the discrete point set (landmarks) w_i can be extracted to correspond to image features [68,69]. Recently, Rohde et al. [29] used RBFs for adaptive image registration, exploiting the fact that RBFs can be arbitrarily distributed, and computational accuracy can be adaptively increased by using denser RBFs at selected regions.

RBFs have also been used in both computer graphics, and engineering. In computer graphics, RBFs and thin-plates splines are used for shape representation [94], shape or image warping [92,95], and animation [96,97]. In engineering, RBFs are the foundation for many meshless methods [98,99], allowing the representation of continuous functions by interpolating scattered node points. These methods are called radial point-interpolation methods (Radial PIM, see [58] for details).

Modeling continuous functions using RBFs present some issues. First, RBFs are essentially global functions, and local deformations result from the linear combination of many RBFs, leading to high computation costs [100]. Secondly, RBFs are unable to reproduce polynomials exactly [58], and produce less accurate results than polynomial models [58]. For example, constant functions $f(\mathbf{x}) = c$, $c \neq 0$ cannot be represented by RBFs [101].

Table 2
Meshless models and methods.

Application areas	Representative works
Point-based computer graphics	Moving Least Squares (MLS) [89], hierarchical partition of unity [88].
Fluid dynamics, simulation	Smoothed-particle hydrodynamics (SPH) [90,91].
Biomedical motion analysis	Meshless deformable model [26–28].

4.3.2. Weighted least-squares (WLS) and partition-of-unity (PU)

Weighted least-squares and partition-of-unity are other type of meshless models for approximating and interpolating continuous functions. For example, smooth surface reconstruction from irregularly distributed sample points was initially studied by Shepard et al. [102]. Shepard's method approximates point sets using locally supported polynomials, and then blend the local polynomial models into a global representation using partition-of-unity [58]. Fig. 8 shows an example of surface approximation. In the figure, the computational domain is divided into cubic regions. Local polynomial models (in red) are constructed from the scattered sample points, and then blended into a global model (in blue). Formally, given a discrete sample set of a function $f(\mathbf{x})$, $\mathbf{x} \in \mathbb{R}^d$, i.e., $(\mathbf{x}_i, f_i), i = 1, 2, \ldots, N$, a polynomial is locally fitted to the data points by minimizing the following functional:

$$\min_{f \in \Pi_m^d} \sum_i \theta(\|\bar{\mathbf{x}}-\mathbf{x}_i\|)\|f(\mathbf{x}_i)-f_i\|^2. \tag{14}$$

Here, $\theta(\|\bar{\mathbf{x}}-\mathbf{x}_i\|)$ is a locally supported *weighting function* or *influence function* that makes the approximation local, while Π_m^d is the space of all polynomials with d variables up to degree m, i.e., a space spanned by multivariate monomials up to degree m. For example, when $m=2$ and $d=2$, we have the space of polynomials $\Pi_m^d = span\{1, x, y, xy, x^2, y^2\}$. If $m=1$ and $d=1$, we have $\Pi_m^d = span\{1, x, y, z\}$. The influence (or weighting) function can be a Gaussian function, $\theta(d) = e^{-\frac{d^2}{h^2}}$, the Wendland function [103], $\theta(d) = \left(1-\frac{d}{h}\right)^4\left(4\frac{d}{h}+1\right)$, or simply the rational function, $\theta(d) = \frac{1}{d^2+\epsilon^2}$, for some $\epsilon > 0$. The theoretical foundation of this local approximation lies in the Taylor's expansion that locally approximates a smooth function using monomials [104]. As a result, the local polynomial model at point $\mathbf{p}$ can be written as a linear combination of monomials. For instance, for $m=2$, $d=2$, we have:

$$f_{\mathbf{p}}(\mathbf{x}) = a_0 + a_1 x + a_2 y + a_3 xy + a_4 x^2 + a_5 y^2 = \mathbf{a}^T \Phi, \tag{15}$$

where $\mathbf{a} = (a_0, \ldots, a_5)^T$, and $\Phi = (1, x, y, xy, x^2, y^2)^T$. Although the order of monomials in the basis vector Φ is not important, in practice, they are arranged according to the Pascal triangle [58], i.e., lower-order monomials precede higher-order ones for better numerical stability. For monomials of the same order, the ones with less difference in the orders of each variable are selected first.

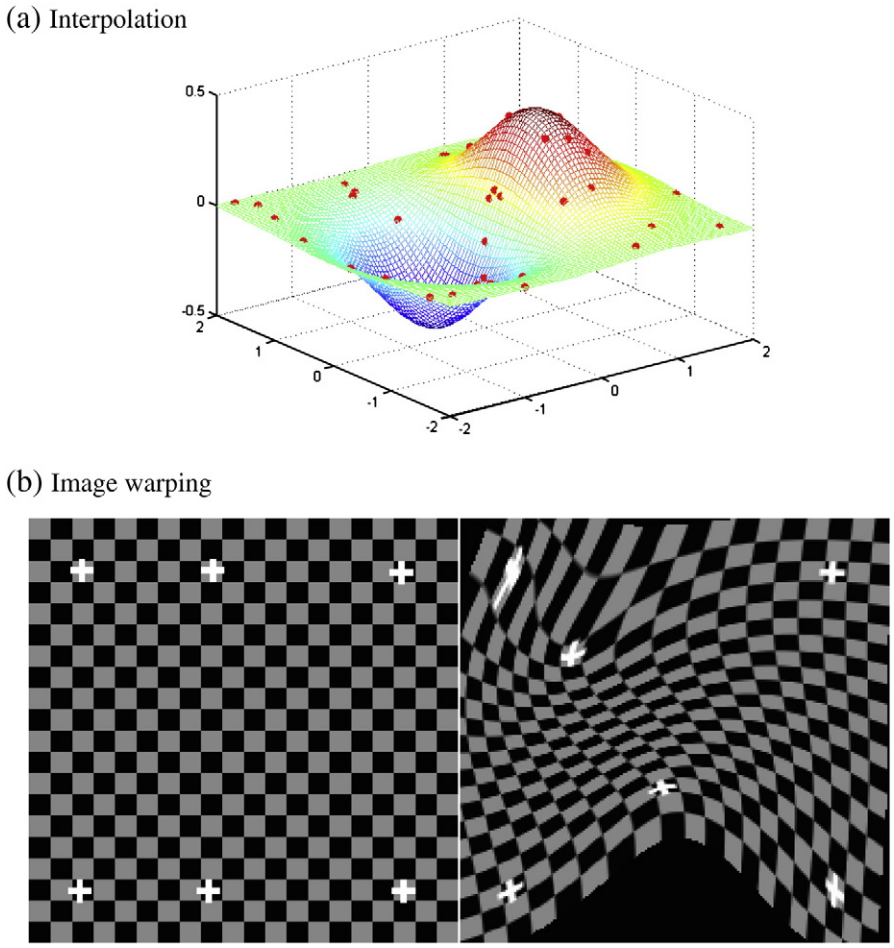

Fig. 7. Applications of radial basis functions. (a) Scattered data interpolation. (b) Nonrigid image warping. Image deformation is blended linearly from the radial basis functions centered at the control points, without relying on the connections between them [92].

After fitting polynomials at discrete positions $\overline{\mathbf{x}}_j, j = 1, \ldots, n$, (i.e., local models) the global deformation model can be assembled by blending the local models. Any point $\mathbf{x}$ in the computational domain Ω might be covered by an arbitrary number of local models, and these models' contribution should sum to one (partition-of-unity). The partition-of-unity function (PU) can be constructed using weight functions θ_j, $j = 1, \ldots, n$. Formally, the blending functions are defined by:

$$\phi_j(\mathbf{x}) = \frac{\theta_j\left(\mathbf{x}-\overline{\mathbf{x}}_j\right)}{\sum_i \theta_i(\mathbf{x}-\overline{\mathbf{x}}_i)}. \tag{16}$$

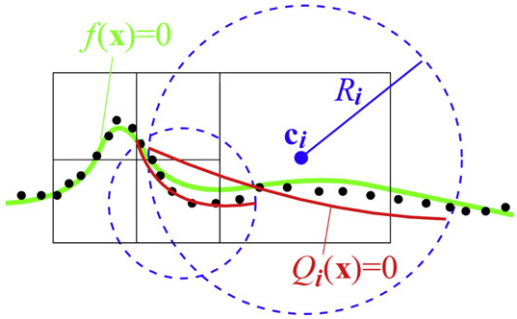

Fig. 8. Surface approximation using WSL and partition-of-unity [100]. The image domain is divided into cubic subregions. In each subregion, local models (red curves) are approximated from scattered sample points, while global model (green curve) is blended from the local models using partition-of-unity.

These functions are also called Shepard's functions [102]. It is easy to verify that $\sum_j \phi_j(\mathbf{x}) = 1$, for $\forall \mathbf{x} \in \Omega$. The global deformation is given by:

$$f(\mathbf{x}) = \sum_j \phi_j(\mathbf{x}) \mathbf{a}_j^T \Phi\left(\mathbf{x}-\overline{\mathbf{x}}_j\right). \tag{17}$$

Recall the B-spline FFD model in Eq. (12) and compare with Eq. (17). It is easy to see that Shepard's method allows local models to overlap with one another, and no explicit neighborhood connection is maintained in Eq. (17). Additionally, the placement of local models can be arbitrary as long as the computational domain Ω is covered by the union of local models' support domains, i.e., $\Omega \subset \cup_j \text{supp}(\theta_j)$.

The key to Shepard's method is the partition-of-unity in Eq. (16) that allows for overlapping of local deformation models. Indeed, Melenk et al. [105] improved finite-element methods by using PU functions to construct overlapping elements, instead of dividing the computational domain into disjoint parts. Similarly to Shepard's method, Melenk also used a monomial basis. Melenk's inspired a large number of applications in engineering. On the other hand, in computer graphics, partition-of-unity and weighted least-squares have been combined with other techniques such as octrees [100,106], and variational methods [107] for point-based shape representation [100] or approximation [107]. In computer vision, similar models have been used for image registration [74,108,109], shape registration [110], and fluid-flow estimation [19].

4.3.3. Moving least-squares (MLS)

Shepard's method was later extended by Lancaster et al. [111] to form an interpolation method called *Moving Least Squares* (MLS). MLS is also based on local weighted least-squares approximation. However, instead of blending together local models centered at discrete points, MLS "moves" the approximation center, and calculates the weighted least-squares fitting at each individual point. As a result, the global deformation function $f(\mathbf{x})$ is obtained as follows:

$$f(\mathbf{x}) = f_{\mathbf{x}}(\mathbf{x}), \quad \min_{f_{\mathbf{x}} \in \Pi_m^d} \sum_i \theta(||\mathbf{x}-\mathbf{x}_i||)||f_{\mathbf{x}}(\mathbf{x}_i)-f_i||^2. \tag{18}$$

As in Shepard's method, MLS does not rely on explicit connections between control points. In addition, MLS has two major features that make it popular in engineering [58,89]: (1) the reconstructed function in Eq. (18) is both continuous and smooth over the entire problem domain when sufficient number of nodes are used; and (2) MLS is capable of reproducing any polynomials up to the degree of the basis monomials. MLS has been widely used in computer graphics for shape representation [88,100,112], animation [59], and physics-based simulation [87]. Due to the natural relationship between computer graphics models and computer vision, there are a number of emerging applications of MLS to vision problems. For example, MLS-based meshless methods have been applied to analyze the motion of a heart's left ventricle [26], feature-based image registration [28,113,114], and 3-D reconstruction [115].

5. Modeling and regularizing continuum motions

In the previous section, we introduced various parametric models for representing continuum deformation fields. However, these models do not provide information about *how* objects deform. For example, based on image data only, there can be many ambiguous solutions leading to local minima in the image-similarity functional (Eq. (1)). As a result, prior information is needed to constraint the solution space. There are three types of prior information used for continuum-motion estimation. First, physics laws and continuum mechanics explain *how* elastic objects or fluid deform. Thus, they can be used to augment image evidence, and provide a *model-driven* approach for motion estimation. On the other hand, continuum-motion models can also be statistically learned from training data, and this can be regarded as a *data-driven* approach. Statistical models are popular in shape reconstruction [116], segmentation [117], or classification [13]. However, they usually do not provide enough accuracy for motion estimation, and for fluid motion, the solution space often has very high number of free-dimensions that prohibit learning of any meaningful statistical model. In this survey, we do not provide further discussion of statistical models. An alternative approach for including prior information is to use simple heuristics. For example, many existing works assume the deformation function to be smooth. Heuristics are often expressed as variational functionals to regularize the deformation field [1,56].

In general, physics models ensure deformation consistency, and are able to produce physically meaningful deformations given initial and boundary conditions [118,119]. Nevertheless, using these models often involves solving higher-order PDEs, that can be computationally expensive [9]. Physics models also make assumptions on material properties such as elasticity, viscosity, and density [118,119], and different models have different admissible objects. Statistical models, on the other hand, make little or no physics assumptions. Instead, prior information is directly learned from training data, and motion estimation is formulated as the problem of maximizing the posterior probability given image evidence [13,117]. A drawback of statistical models is their need to be trained beforehand, and that ground-truth training data can be difficult to obtain. Finally, the use of heuristics can be considered as a *weaker* prior than physics and statistical models, as they only make very general assumptions about the deformation [6,9,120]. Smoothness heuristics can be simple and efficient, but they are also more sensitive to image noise and outliers.

It is worth pointing out that the boundary between these approaches to solution regularization is not always clear. For instance, in medical imaging [10,121], fluid-registration methods use fluid-dynamics models as heuristics to regulate large image deformation, although the target objects (human organs) are generally not fluid. Also, statistical priors can be combined with smoothness heuristics [122], leading to improved robustness, and they can also be used to estimate material parameters for physics models. Finally, some smoothness regularizers have physical meanings, e.g., thin-plate energy.

5.1. Physics and continuum mechanics models

Physics and continuum mechanics provide natural prior information for continuum motion, based on fundamental physical laws [119] such as the conservation of mass, conservation of momentum, and conservation of energy. By applying these laws to fluid or elastic objects, differential equations can be derived to describe their dynamic behavior. In Section 3, we have already discussed the application of mass constancy in both fluid [6] and elastic objects [36]. These applications, however, only use the relationship between the deformation's divergence and image-intensity variation, and this relationship is not related to the objects' dynamics. In this section, we introduce two of the most popular models in continuum-motion estimation, namely, the elastic solid mechanics model, and the fluid Navier–Stokes equations [123].

5.1.1. Elastic solid mechanics

Elastic models have been used in nonrigid image registration and computer graphics for many years [124,125], and they are popular in medical imaging applications [2,126,127]. In fact, medical imaging is mostly concerned with elastic biological tissues, and the modeling of these tissues using elastic-solid mechanics is an important subject in biomechanics [70]. Due to the large amount of work using elastic-physics models, our survey focuses on the most typical assumptions and applications.

Most elastic models assume the source image to be an isotropic-elastic continuum with linear elasticity, i.e., the material stress is proportional to its local infinitesimal deformation (i.e., strain). Formally, the strain tensor ϵ can be calculated from the divergence of the deformation, i.e., $\epsilon = \frac{1}{2}\left[\nabla\mathbf{u} + (\nabla\mathbf{u})^T\right]$, and the stress tensor σ is the inner product of the constant material stiffness tensor $\mathbf{C}$ and the strain tensor, $\sigma = \mathbf{C}\cdot\epsilon$ (Hooke's law). The 1-D case of the linear elasticity is equivalent to the deformation of a spring.

For motion estimation, elastic models are often used in two different ways. On one hand, the elastic potential $\int_\Omega \sigma^T \epsilon \, d\Omega$ can be used as a regularizer [70,128,129] to penalize undesired variations in the estimated deformation field. In this case, elastic models are usually combined with a data term describing the similarity between the warped source image and the target image, and the deformation field is obtained by minimizing a variational functional. As discussed in Section 3, the similarity measure can be squared-sum-of-differences (SSD) [70,129] or the mutual information (MI) [31,38,73].

On the other hand, elastic models can also be used to propagate deformation from landmarks' motion, where correspondences of landmarks or image features are given as boundary conditions. Then, a dense deformation field is obtained by solving the *equilibrium equations* [130,131] (also called Lagrangian equations [26,27]), instead of solving the inverse problem directly. Some existing works use image evidence as external forces [132], but many others only select a sparse set of salient features as landmarks, obtain their correspondences, and enforce the correspondences as boundary conditions to

the equilibrium equations [26,27,130,131]. Generally speaking, this approach is a direct extension of the methods used in both mechanics engineering and computer graphics.

5.1.2. Navier–Stokes equations

The Navier–Stokes equations describe the motion of fluid substances, and they are derived from the law of momentum conservation, together with the assumption that the fluid stress is the sum of a diffusing viscous term, plus a pressure term [118]. Formally, a basic form of the equation is given by:

$$\rho\frac{D\mathbf{v}}{Dt} = -\Delta p + \Delta\cdot\mathbb{T} + \mathbf{f}, \tag{19}$$

where $\mathbf{v}$ is the velocity field, ρ is the fluid density, p is the pressure, $\mathbb{T}$ is the stress tensor, and $\mathbf{f}$ represents the body forces. The physical meaning of Eq. (19) is straightforward. On the left-hand side, $\frac{D\mathbf{v}}{Dt}$ describes the fluid acceleration, and the right-hand side of the equation is the summation of the body forces and divergence of stress (i.e., pressure p and shear stress $\mathbb{T}$). The basic form in Eq. (19) has many variants for different types of fluids (see [118,119] for more details).

The Navier–Stokes' equations and their variants have been used in fluid-motion estimation. For example, Cuzol et al. [3,133] represented fluid flows with a sparse set of singular points (i.e., vortices and sources). These singular points form the boundary conditions for the flow field, and the dense fluid motion can be efficiently estimated or tracked, by solving the Navier–Stokes equations. Motion estimation can also be formulated as a filtering or an optimal control problems [134,135]. In this case, Navier–Stokes' equations become the system equations, while the image evidence is used as feedback.

Navier–Stokes equations are also used for registering medical images undergoing large deformations [10,121]. Here, the source image is modeled as a viscous fluid, and gradually deformed into the target image. Unlike the elastic solid model that penalizes local deformation proportionally to its magnitude, Navier–Stokes equations are not biased towards small deformations, yet they still ensure spatially smooth deformations. As for some elastic solid models, image evidence provides external forces, i.e., $\mathbf{f}$ in Eq. (19). For example, Christensen [10] proposed the first nonrigid image registration method based on fluid dynamics, where the external force is derived from image gradients. Agostino et al. [121] extended this work to 3-D, and derived the external force from mutual information.

5.2. Smoothness regularizers

In many motion-estimation problems, high accuracy can be achieved by simply regulating the deformation's smoothness. Horn et al. [1] proposed the classic smoothness regularizer for optical-flow estimation. Horn–Schunck's optical-flow estimation method can be formulated as the minimization of the following functional:

$$E = \underbrace{\int_\Omega \|I'(\mathbf{x}+\mathbf{u}) - I(\mathbf{x})\|^2 d\mathbf{x}}_{\text{Data Term}} + \underbrace{\lambda\int_\Omega \left(\left\|\frac{\partial\mathbf{u}}{\partial x}\right\|^2 + \left\|\frac{\partial\mathbf{u}}{\partial y}\right\|^2,\right) d\mathbf{x}}_{\text{Regularizer}}, \tag{20}$$

where the regularizer penalizes the deformation field's spatial variation, and λ controls the relative importance of the regularizer. Horn–Schunck's regularizer has two problems. First, it does not handle outliers robustly, and thus tends to over-smooth motion boundaries for general optical-flow computation. However, this is not a serious problem for continuum motion, and can be addressed using robust statistics [30], or changing the regularizer to the L^1 norm [52]. Secondly, Horn–Schunck's regularizer is biased towards piecewise-constant deformations, as this one is indeed the only deformation field that makes the regularizer term vanish.

There are two higher-order regularizers commonly used in continuum-motion estimation. For elastic solids, the most commonly used regularizer is based on second-order derivatives. In 2-D, this regularizer takes the following form [56]:

$$C_{smooth} = \int_\Omega\int \left[\left(\frac{\partial^2\mathbf{u}}{\partial x^2}\right)^2 + \left(\frac{\partial^2\mathbf{u}}{\partial y^2}\right)^2 + 2\left(\frac{\partial^2\mathbf{u}}{\partial xy}\right)^2\right] dxdy. \tag{21}$$

The regularizer in Eq. (21) is not biased to piecewise-constant deformations, and it resembles the stress energy of an elastic thin-plate [68]. In the case of fluids, a second-order regularizer can be defined by penalizing the spatial variation of the deformation's divergence and rotation [6], i.e.,

$$C_{smooth} = \int_\Omega \left(\|\nabla \mathrm{div}\ \mathbf{u}\|^2 + \|\nabla \mathrm{rot}\ \mathbf{u}\|^2\right) d\mathbf{x}. \tag{22}$$

This regularizer was first used for data approximation [136], using so called vector-splines. Suter et al. [22] extended it for optical-flow computation, and then it was applied to fluid-motion estimation by Corpetti et al. [6,20]. Some recent works on fluid-motion estimation also use this regularizer [9,19,120]. Meanwhile, the vector-spline regularizer was used in medical image registration [137,138].

6. Quantitative evaluation

In the previous sections, we have reviewed many existing methods for estimating continuum motion, and compared their strengthens and weaknesses. However, we did not comment on the problem of how to quantitatively evaluate these methods. Extensive quantitative evaluation that includes all motion estimation methods is difficult to obtain due to a number of reasons. In this section, we first introduce the challenges in evaluating continuum-motion estimation methods, and then we summarize existing evaluation methodologies and approaches.

6.1. Challenges in quantitative evaluations

First, the performance of a motion-estimation method depends on all of its three components: similarity measure, deformation model, and regularizer or prior information. It is difficult to single out the contribution of individual components, and finding the best combination of these components is still an unsolved problem. Thus, it is common for researchers to limit the scope of their evaluation by fixing components of the compared methods. For example, Penny et al. [139] compared six similarity measures used in 3-D to 2-D image registration, by limiting the deformation to a rigid transformation.

Secondly, there are many intertwined and even conflicting goals in designing motion-estimation algorithms. For example, trade-offs between computational efficiency and accuracy are common. Furthermore, depending on the application, there are other designing goals that are equally desirable, and sometimes even more important. In medical image registration for instance, the ability to produce diffeomorphic deformations is indispensable for computational anatomy [140], despite the fact that diffeomorphic registration methods may produce less-accurate results [141] in comparison with their non-diffeomorphic counterparts.

Finally, the problem of continuum-motion estimation includes a large range of applications. Even though the general principles of continuum motions apply, one still faces different challenges in each application as well as the need to use datasets of different nature. In medical image registration, it is well known that performance of registration methods varies with image modalities (e.g., MRI and CT)

and the type of registered objects (e.g., brain, breast, and lungs) [2,39]. Similarly, fluid-motion estimation methods that perform well on PIV images may produce poor results on satellite images [6,17].

Due to these challenges, quantitative evaluations of continuum motions often focus on specific applications and datasets [17,141], that are worthy dedicating an entire paper [141–143] to describe their evaluation methodologies, datasets, and settings. In this survey, we find it more helpful and plausible to provide a road-map for future investigation, by summarizing existing evaluation methodologies and datasets, instead of attempting to provide a single universal evaluation.

6.2. Methodologies and datasets

Existing quantitative-evaluation methodologies can be classified into direct and indirect methods, depending on the availability and usage of ground-truth data. If ground-truth motion data is available, then the estimated motion can be directly compared with it. However, obtaining ground-truth data for real-world motions is notoriously difficult. Thus, researchers sometimes resort to simulated image sequences where motion data is readily available [144,145]. Still, synthetic datasets are rather limited and simplistic in comparison with real-world applications, so they are commonly used for baseline evaluation. In this case, many error metrics can be used to measure the estimation results' accuracy, such as the classic L_1 and L_2 metrics [17], and the angular and end-point error used in optical-flow benchmark evaluations [51].

In many other cases, ground-truth motion data is not available, but comparison of estimation methods can still be performed based on some high-level indirect measurement, especially when motion estimation is used as a preprocessing step. For example, in medical image registration, the estimated deformation is often used to propagate image segmentation labels from a template image to the registered target images. Then, motion-estimation results can be evaluated by the quality of propagated labels, according to the percentage of overlapping between the propagated segmentations and the manually labeled ground-truth segmentations [141,142,159]. Motion estimation results can also be indirectly evaluated according to their applications in object recognition [160], or feature tracking [3,156]. In Table 3, we compiled a list of popular datasets for evaluating continuum-motion estimation methods together with some representative evaluations performed on those datasets. This table is by no means a complete list of all available datasets, but provides a broad view of such resources and applications that should be useful for those who are embarking in the study of this rich subject.

7. Discussion and conclusion

In the previous sections, we provided a review of continuum-motion estimation methods. Despite the large number of existing works in continuum-motion estimation and analysis, there are still many open problems. We would like to conclude this survey bypointing out a number of possible directions for future study. To summarize, these directions are:

1. Diffeomorphic motion estimation.
2. Motion estimation with missing or partial data.
3. GPU-based real-time motion estimation.
4. Validation and benchmarking of motion estimation algorithms.

Most existing works on continuum-motion estimation are focused on producing smooth deformation fields. Emerging applications such as computational anatomy [161] requires the deformation field to be not only smooth, but also *invertible* [162]. In other words, the nonrigid mapping is *diffeomorphic*, and there is an one-to-one correspondence between the source image and the deformed target image. Recently, diffeomorphism has been mainly studied in the context of medical image registration [140,147,159,162]. Rueckert et al. [162] extended the B-spline-based registration method [56], and produced invertible registration results, by enforcing the deformation field's Jacobian matrix to be positive-definite. Ashburner [159] extended fluid-registration methods [10,121] by using an *invertible fluid dynamic* system to regulate the deformation field. Following these ideas, it is interesting to see how diffeomorphism can be enforced in other existing registration methods, especially meshless methods [29,74].

In clinical practice, medical image registration algorithms may have to work with images with missing or partial data due to image noise, occlusion, and other clinical conditions [163]. Most existing works use variational methods with robust kernel functions [163] to reduce the influence of outliers, or train a statistical model from ground-truth data [146]. Variational methods are less robust and less efficient than their statistical counterparts, while statistical methods require large amount of training data which are expensive to obtain. A promising direction might be to combine the variational framework with statistical models. Thus, the robustness of variational methods can be improved, while training requirements of statistical models can be reduced.

A common drawback of recent nonrigid motion estimation methods is their high computational cost, limiting their usage in real-time and interactive applications. With the development of graphics processing unit (GPU), many vision computations can be implemented as parallel algorithms running on affordable consumer graphics cards. Zach et al. [52] implemented a real-time optical-flow algorithm based on GPU. Parallel implementations of nonrigid image registration algorithms are even more appealing since most registration algorithms are concerned with 3-D image data that demand more computational power [164–166]. GPU implementation of fluid-motion estimation algorithms have been mostly focused on classic window-based cross-correlation methods [167], and little attention has been given to recent variational methods that produce state-of-the-art results.

Finally, despite the large number of studies in nonrigid image registration and fluid motion estimation, evaluation methods and

Table 3
Public available datasets for quantitative evaluation.

Dataset	Description and evaluations
BrainWeb [144]	3-D brain MRI images undergo simulated deformations. Fluid registration [121], spline models [146], and diffeomorphic Demons [147].
YORKU [148]	3-D cardiac MRI image sequences. Meshless [109] and polynomial models [54]
Visible Human [149]	CT images and 3-D human body models. Biomechanical models for registration [150] and simulation [151,152]
LPBA40 [153]	Brain MRI data with manually labeled segmentations. Volume-based and surface-based registration [141,143].
EUMETSAT[a]	Satellite images obtained from both visible- and invisible-channel sensors. Second-order regularizer [6], and vector-spline model [9].
PIV-STD [145]	3-D synthetic PIV images. Variational fluid-motion estimation [17]. Physics-based spatial–temporal regularization [154].
FLUID[b]	Synthetic and experimental PIV image sequences. Fluid tracking [133] and vector-spline model [9].
MMI[c] [155]	2-D facial expression image sequences. Robust estimators for tracking facial expressions [41]. FFD-based surface registration [156].
BU-4DFE [157]	3-D range data with color texture of facial expressions. 3-D face tracking based on mesh models [158].

[a] http://www.eumetsat.int/.
[b] http://www.fluid.irisa.fr.
[c] http://www.mmifacedb.com/.

benchmarks for comparing different algorithms are relatively limited. On one hand, ground-truth data for nonrigid motion estimation is difficult to obtain. As a result, many researchers use synthetic images for evaluation [9,168,169]. On the other hand, due to the large number of different applications of motion estimation, many algorithms were evaluated in different context with different goals [170]. For example, in medical imaging, registration algorithms have been evaluated in the tasks of segmentation [57], deformation predication [159], and classification [146]. There have been recent efforts for providing a unified evaluation framework and dataset for nonrigid registration methods [142,169]. However, datasets are still mostly synthetic, and the availability of a dataset containing real-world ground-truth, like the one available for optical-flow computation [51], is highly desirable.

References

[1] B.K.P. Horn, B.G. Schunck, Determining optical flow, Artificial Intelligence 17 (1–3) (August 1981) 185–203.
[2] J.B. Maintz, M.A. Viergever, A survey of medical image registration, Medical Image Analysis 2 (1) (1998) 1–36.
[3] A. Cuzol, P. Hellier, E. Memin, A low dimensional fluid motion estimator, International Journal of Computer Vision 75 (3) (December 2007) 329–349.
[4] A. Mitiche, P. Bouthemy, Computation and analysis of image motion: A synopsis of current problems and methods, International Journal of Computer Vision 19 (1) (1996) 29–55.
[5] T.B. Moeslund, E. Granum, A survey of computer vision-based human motion capture, Computer Vision and Image Understanding 81 (3) (2001) 231–268.
[6] T. Corpetti, É. Mémin, P. Pérez, Dense estimation of fluid flows, IEEE Transaction on Pattern Analysis and Machine Intelligence 24 (3) (2002) 365–380.
[7] R. Eils, C. Athale, Computational imaging in cell biology, Journal of Cell Biology 161 (3) (2003) 477–481.
[8] T.B. Moeslund, A. Hilton, V. Krüger, A survey of advances in vision-based human motion capture and analysis, Computer Vision and Image Understanding 104 (2) (2006) 90–126.
[9] T. Isambert, J.P. Berroir, I. Herlin, A multi-scale vector spline method for estimating the fluids motion on satellite images, European Conference on Computer Vision, 2008, pp. 665–676.
[10] G.E. Christensen, R.D. Rabbitt, M.I. Miller, Deformable templates using large deformation kinematics, IEEE Transactions on Image Processing 5 (10) (1996) 1435–1447.
[11] A. Gholipour, N. Kehtarnavaz, R. Briggs, M. Devous, K. Gopinath, Brain functional localization: A survey of image registration techniques, IEEE Transactions on Medical Imaging 26 (4) (2007) 427–451.
[12] E.T. Bullmore, M.J. Brammer, S. Rabe-Hesketh, V.A. Curtis, R.G. Morris, S.C.R. Williams, T. Sharma, P.K. McGuire, Methods for diagnosis and treatment of stimulus-correlated motion in generic brain activation studies using fMRI, Human Brain Mapping 7 (1) (1999) 38–48.
[13] R. Chandrashekara, A. Rao, G. Sanchez-Ortiz, R. Mohiaddin, D. Rueckert, Construction of a statistical model for cardiac motion analysis using nonrigid image registration, Information Processing in Medical Imaging, 2003, pp. 599–610.
[14] S. Klein, U.A. van der Heide, B.W. Raaymakers, A. Kotte, M. Staring, J.P.W. Pluim, Segmentation of the prostate in MR images by atlas matching, 4th IEEE International Symposium on Biomedical Imaging: From Nano to Macro, 2007, pp. 1300–1303.
[15] D. Decarlo, D. Metaxas, Optical flow constraints on deformable models with applications to face tracking, International Journal of Computer Vision 38 (2) (2000) 99–127.
[16] J. Schnabel, C. Tanner, A. Castellano Smith, D. Hill, D. Hawkes, M. Leach, C. Hayes, A. Degenhard, R. Hose, Validation of non-rigid registration using finite element methods, Information Processing in Medical Imaging, 2001, pp. 344–357.
[17] D. Heitz, E. Mémin, C. Schnórr, Variational fluid flow measurements from image sequences: synopsis and perspectives, Experiments in Fluids 48 (3) (2009) 369–393.
[18] L. Alvarez, C. Castaño, M. García, K. Krissian, L. Mazorra, A. Salgado, J. Sánchez, A variational approach for 3D motion estimation of incompressible PIV flows, Scale Space and Variational Methods in Computer Vision, 2010, pp. 837–847.
[19] T. Isambert, J.P. Berroir, I. Herlin, L.C. Inria, Fast and stable vector spline method for fluid apparent motion estimation, IEEE International Conference on Image Processing, 2007, pp. 505–508.
[20] T. Corpetti, E. Mémin, P. Pérez, Estimating fluid optical flow, International Conference on Pattern Recognition, 2000, pp. 1033–1036.
[21] K.Y. Wong, C.L. Yip, Identifying centers of circulating and spiraling vector field patterns and its applications, Pattern Recognition 42 (7) (2009) 1371–1387.
[22] D. Suter, Motion estimation and vector splines, IEEE Conference on Computer Vision and Pattern Recognition, 1994, pp. 939–942.
[23] K.K.L. Wong, R.M. Kelso, S.G. Worthley, P. Sanders, J. Mazumdar, D. Abbott, Theory and validation of magnetic resonance fluid motion estimation using intensity flow data, PLoS ONE 4 (3) (2009) e4747 March.
[24] B. Zitová, J. Flusser, Image registration methods: a survey, Image and Vision Computing 21 (11) (October 2003) 977–1000.
[25] M. Holden, A review of geometric transformations for nonrigid body registration, IEEE Transactions on Medical Imaging 27 (1) (2008) 111–128.
[26] X. Wang, T. Chen, S. Zhang, D. Metaxas, L. Axel, Lv motion and strain computation from TMRI based on meshless deformable models, Medical Image Computing and Computer-Assisted Intervention, 2008, pp. 636–644.
[27] T. Chen, X. Wang, D. Metaxas, L. Axel, Fast motion tracking of tagged MRI using angle-preserving meshless registration, Medical Image Computing and Computer-Assisted Intervention, 2008, pp. 313–320.
[28] H. Liu, P. Shi, Meshfree particle method, IEEE International Conference on Computer Vision, 2003, pp. 289–296.
[29] G.K. Rohde, A. Aldroubi, B.M. Dawant, The adaptive bases algorithm for intensity-based nonrigid image registration, IEEE Transactions on Medical Imaging 22 (11) (2003) 1470–1479.
[30] T. Brox, A. Bruhn, N. Papenberg, J. Weickert, High accuracy optical flow estimation based on a theory for warping, European Conference on Computer Vision, 2004, pp. 25–36.
[31] J.P.W. Pluim, J.B.A. Maintz, M.A. Viergever, Mutual-informationbased registration of medical images: a survey, IEEE Transactions on Medical Imaging 22 (8) (2003) 986–1004.
[32] P. Viola, W.M. Wells III, Alignment by maximization of mutual information, International Journal of Computer Vision 24 (2) (1997) 137–154.
[33] Z. Yi, S. Soatto, Nonrigid registration combining global and local statistics, IEEE Conference on Computer Vision and Pattern Recognition, 2009, pp. 2200–2207.
[34] R.P. Wildes, M.J. Amabile, A.M. Lanzillotto, T.S. Leu, Recovering estimates of fluid flow from image sequence data, Computer Vision and Image Understanding 80 (2) (2000) 246–266.
[35] V. Devlaminck, A functional for compressible or incompressible elastic deformation estimation, IEEE Signal Processing Letters 6 (7) (1999) 162–164.
[36] E. Castillo, R. Castillo, Y. Zhang, T. Guerrero, Compressible image registration for thoracic computed tomography images, Journal of Medical and Biological Engineering 29 (5) (2009) 222–233.
[37] Y. Yin, E.A. Hoffman, C.L. Lin, Mass preserving nonrigid registration of CT lung images using cubic B-spline, Medical Physics 36 (9) (2009) 4213–4222.
[38] F. Maes, D. Vandermeulen, P. Suetens, Medical image registration using mutual information, Proceedings of the IEEE 91 (10) (2003) 1699–1722.
[39] D.L.G. Hill, P.G. Batchelor, M. Holden, D.J. Hawkes, Medical image registration, Physics in Medicine and Biology 46 (3) (2001) 1–45.
[40] A. Myronenko, X. Song, Intensity-based image registration by minimizing residual complexity, IEEE Transaction on Medical Imaging 29 (11) (November 2010) 1882–1891.
[41] M. Pantic, I. Patras, Dynamics of facial expression: Recognition of facial actions and their temporal segments from face profile image sequences, IEEE Transactions on Systems, Man, and Cybernetics, Part B: Cybernetics 36 (2) (2006) 433–449.
[42] B. Brendel, S.W.A. Rick, M. Stockheim, H. Ermert, Registration of 3D CT and ultrasound datasets of the spine using bone structures, Computer Aided Surgery 7 (3) (2002) 146–155.
[43] K.A. Vermeer, F.M. Vos, H.G. Lemij, A.M. Vossepoel, A model based method for retinal blood vessel detection, Computers in Biology and Medicine 34 (3) (2004) 209–219.
[44] M. Thomas, S. Misra, C. Kambhamettu, J.T. Kirby, A robust motion estimation algorithm for PIV, Measurement Science and Technology 16 (3) (2005) 865–877.
[45] D. Shen, C. Davatzikos, HAMMER: hierarchical attribute matching mechanism for elastic registration, IEEE Transactions on Medical Imaging 21 (11) (2002) 1421–1439.
[46] H. Shekarforoush, M. Berthod, J. Zerubia, Subpixel image registration by estimating the polyphase decomposition of cross power spectrum, IEEE Conference on Computer Vision and Pattern Recognition, 1996, pp. 532–537.
[47] J.Z. Wang, L.E. Reinstein, J. Hanley, A.G. Meek, Investigation of a phase-only correlation technique for anatomical alignment of portal images in radiation therapy, Physics in Medicine and Biology 41 (6) (1996) 1045–1058.
[48] J. Kim, J.A. Fessler, Intensity-based image registration using robust correlation coefficients, IEEE Transactions on Medical Imaging 23 (11) (2004) 1430–1444.
[49] A. Roche, X. Pennec, G. Malandain, N. Ayache, Rigid registration of 3-D ultrasound with MR images: a new approach combining intensity and gradient information, IEEE Transactions on Medical Imaging 20 (10) (2001) 1038–1049.
[50] M.J. Black, P. Anandan, The robust estimation of multiple motions: Parametric and piecewise-smooth flow fields, Computer Vision and Image Understanding 63 (1) (1996) 75–104.
[51] S. Baker, S. Roth, D. Scharstein, M.J. Black, J.P. Lewis, R. Szeliski, A database and evaluation methodology for optical flow, IEEE International Conference on Computer Vision, 2007, pp. 1–8.
[52] T. Pock, M. Urschler, C. Zach, R. Beichel, H. Bischof, A duality based algorithm for TV-L1-optical-flow image registration, Medical Image Computing and Computer-Assisted Intervention, Springer, 2007, pp. 511–518.
[53] T. Nir, A.M. Bruckstein, R. Kimmel, Over-parameterized variational optical flow, International Journal of Computer Vision 76 (2) (2008) 205–216.
[54] W. Liu, E. Ribeiro, Estimating nonrigid shape deformation using moments, IEEE International Conference on Pattern Recognition, 2010, pp. 185–188, August.
[55] M.D. Buhmann, Radial basis functions: theory and implementations, Cambridge University Press, Cambridge, 2003.
[56] D. Rueckert, L.I. Sonoda, C. Hayes, D.L.G. Hill, M.O. Leach, D.J. Hawkes, Nonrigid registration using free-form deformations: application to breast MR images, IEEE Transactions on Medical Imaging 18 (8) (1999) 712–721.
[57] M.S. Hansen, R. Larsen, D. Lyngby, B. Glocker, N. Navab, G. München, Adaptive parametrization of multivariate B-splines for image registration, IEEE Conference on Computer Vision and Pattern Recognition, 2008, pp. 1–8.

[58] G.R. Liu, Meshfree methods: moving beyond the finite element method, 2nd Edition CRC, 2009 July.
[59] L. Kobbelt, M. Botsch, A survey of point-based techniques in computer graphics, Computers & Graphics 28 (6) (2004) 801–814.
[60] H. Wendland, Scattered data approximation, Cambridge University Press, Cambridge, 2005.
[61] R.Y. Tsai, T.S. Huang, Uniqueness and estimation of threedimensional motion parameters of rigid objects with curved surfaces, IEEE Transactions on Pattern Analysis and Machine Intelligence 6 (1) (1984) 13–27.
[62] A. Ravishankar Rao, Ramesh C. Jain, Computerized flow field analysis: Oriented texture fields, IEEE Transaction on Pattern Analysis and Machine Intelligence 14 (7) (1992) 693–709.
[63] C.F. Shu, R.C. Jain, Vector field analysis for oriented patterns, IEEE Transaction on Pattern Analysis and Machine Intelligence 16 (9) (1994) 946–950.
[64] P. Ruhnau, T. Kohlberger, C. Schnórr, H. Nobach, Variational optical flow estimation for particle image velocimetry, Experiments in Fluids 38 (1) (2005) 21–32.
[65] D. Cremers, S. Soatto, Motion competition: A variational approach to piecewise parametric motion segmentation, International Journal of Computer Vision 62 (3) (2005) 249–265.
[66] J. Hoey, J.J. Little, Bayesian clustering of optical flow fields, IEEE International Conference on Computer Vision, 2003, pp. 1086–1093.
[67] O. Kihl, B. Tremblais, B. Augereau, Multivariate orthogonal polynomials to extract singular points, IEEE International Conference on Image Processing, 2008, pp. 857–860.
[68] C.R. Meyer, J.L. Boes, B. Kim, P.H. Bland, K.R. Zasadny, P.V. Kison, K. Koral, K.A. Frey, R.L. Wahl, Demonstration of accuracy and clinical versatility of mutual information for automatic multimodality image fusion using affine and thin-plate spline warped geometric deformations, Medical Image Analysis 1 (3) (1997) 195–206.
[69] K. Rohr, H.S. Stiehl, R. Sprengel, T.M. Buzug, J. Weese, M.H. Kuhn, Landmark-based elastic registration using approximating thinplate splines, IEEE Transactions on Medical Imaging 20 (6) (2001) 526–534.
[70] M. Ferrant, S. Warfield, A. Nabavi, F. Jolesz, R. Kikinis, Registration of 3D intraoperative MR images of the brain using a finite element biomechanical model, Medical Image Computing and Computer-Assisted Intervention, 2000, pp. 249–258.
[71] J.A. Schnabel, C. Tanner, A.D. Castellano-Smith, A. Degenhard, M.O. Leach, D.R. Hose, D.L.G. Hill, D.J. Hawkes, Validation of nonrigid image registration using finite-element methods: application to breast MR images, IEEE Transactions on Medical Imaging 22 (2) (2003) 238–247.
[72] A. Bharatha, M. Hirose, N. Hata, S.K. Warfield, M. Ferrant, K.H. Zou, E. Suarez-Santana, J. Ruiz-Alzola, A. D'Amico, R.A. Cormack, et al., Evaluation of three-dimensional finite element-based deformable registration of pre-and intraoperative prostate imaging, Medical Physics 28 (12) (2001) 2551–2560.
[73] K.K. Brock, M.B. Sharpe, L.A. Dawson, S.M. Kim, D.A. Jaffray, Accuracy of finite element model-based multi-organ deformable image registration, Medical Physics 32 (6) (2005) 1647–1659.
[74] S. Makram-Ebeid, O. Somphone, Non-rigid image registration using a hierarchical partition of unity finite element method, IEEE International Conference on Computer Vision, 2007, pp. 1–7.
[75] E.G. Kahn. Computational strategies for meshfree nonrigid registration. PhD thesis, Yale University, December 2006.
[76] G. Farnebáck, C.F. Westin, Affine and deformable registration based on polynomial expansion, Medical Image Computing and Computer-Assisted Intervention, 2006, pp. 857–864.
[77] X. Pennec, N. Ayache, A. Roche, P. Cachier, Non-rigid MR/US registration for tracking brain deformations, IEEE International Workshop on Medical Imaging and Augmented Reality, 2001, pp. 79–86.
[78] S. Zachow, Modellierung von Weichgewebe - Simulation von Deformation und Destruktion - Neue Möglichkeiten in der computergestützten Chirurgie, Shaker Verlag, 1998.
[79] S. Klein, M. Staring, K. Murphy, M.A. Viergever, J.P.W. Pluim, elastix: a toolbox for intensity-based medical image registration, IEEE Transactions on Medical Imaging 29 (1) (2010) 196–205.
[80] D. Salomon, Curves and surfaces for computer graphics, Springer-Verlag New York Inc., 2006.
[81] N. Amenta, M. Bern, M. Kamvysselis, A new Voronoi-based surface reconstruction algorithm, Proceedings of the 25th Annual Conference on Computer Graphics and Interactive Techniques, 1998, pp. 421–427.
[82] S. Bischoff, D. Pavic, L. Kobbelt, Automatic restoration of polygon models, ACM Transactions on Graphics 24 (4) (2005) 1332–1352.
[83] W. Welch, A. Witkin, Free-form shape design using triangulated surfaces, Proceedings of the 21st Annual Conference on Computer Graphics and Interactive Techniques, 1994, pp. 247–256.
[84] L.P. Kobbelt, T. Bareuther, H.P. Seidel, Multiresolution shape deformations for meshes with dynamic vertex connectivity, Computer Graphics Forum 19 (3) (2000) 249–260.
[85] S. Kim, S. Park, W. Jung, H. Shin, Progressive Model Construction for N-Sided Polygonal Meshes, IJCC Workshop on Digital Engineering, 2006, pp. 203–210.
[86] Y. Zhang, C. Bajaj, B.S. Sohn, 3D finite element meshing from imaging data, Computer Methods in Applied Mechanics and Engineering 194 (48–49) (2005) 5083–5106.
[87] A. Nealen, M. Muller, R. Keiser, E. Boxerman, M. Carlson, Physically based deformable models in computer graphics, Computer Graphics Forum 25 (4) (2006) 809–836.
[88] M. Alexa, J. Behr, D. Cohen-Or, S. Fleishman, D. Levin, C.T. Silva, Computing and rendering point set surfaces, IEEE Transactions on Visualization and Computer Graphics 9 (1) (2003) 3–15.
[89] D. Levin, The approximation power of moving least-squares, Mathematics of Computation 67 (224) (1998) 1517–1531.
[90] M.B. Liu, Smoothed particle hydrodynamics: a meshfree particle method, World Scientific Publishing Company, 2003.
[91] F. Petronetto, A. Paiva, M. Lage, G. Tavares, H. Lopes, T. Lewiner, Meshless Helmholtz-Hodge decomposition, IEEE Transactions on Visualization and Computer Graphics 16 (2) (2009) 338–349.
[92] N. Arad, N. Dyn, D. Reisfeld, Y. Yeshurun, Image warping by radial basis functions: application to facial expressions, Graphical Models and Image Processing 56 (2) (1994) 161–172.
[93] F.L. Bookstein, Principal warps: Thin-plate splines and the decomposition of deformations, IEEE Transaction on Pattern Analysis and Machine Intelligence 11 (6) (1989) 567–585.
[94] J.C. Carr, R.K. Beatson, J.B. Cherrie, T.J. Mitchell, W.R. Fright, B.C. McCallum, T.R. Evans, Reconstruction and representation of 3D objects with radial basis functions, Proceedings of the 28th Annual Conference on Computer Graphics and Interactive Techniques, 2001, pp. 67–76.
[95] M. Botsch, L. Kobbelt, Real-time shape editing using radial basis functions, Computer Graphics Forum 24 (3) (2005) 611–622.
[96] J. Noh, D. Fidaleo, U. Neumann, Animated deformations with radial basis functions, Proceedings of the ACM Symposium on Virtual Reality Software and Technology, 2000, pp. 166–174.
[97] C.F. Rose, P.P.J. Sloan, M.F. Cohen, Artist-directed inversekinematics using radial basis function interpolation, Computer Graphics Forum 20 (3) (2001) 239–250.
[98] H. Wendland, Meshless Galerkin methods using radial basis functions, Mathematics of Computation 68 (228) (1999) 1521–1531.
[99] J.G. Wang, G.R. Liu, On the optimal shape parameters of radial basis functions used for 2-D meshless methods, Computer Methods in Applied Mechanics and Engineering 191 (23–24) (2002) 2611–2630.
[100] Y. Ohtake, A. Belyaev, M. Alexa, G. Turk, Seidel Hans-Peter, Multi-level partition of unity implicits, ACM Transaction of Graphics 22 (3) (2003) 463–470.
[101] J.G. Wang, G.R. Liu, A point interpolation meshless method based on radial basis functions, International Journal for Numerical Methods in Engineering 54 (11) (2002) 1623–1648.
[102] D. Shepard, A two-dimensional interpolation function for irregularlyspaced data, Proceedings of the 23rd ACM National Conference, 1968, pp. 517–524.
[103] H. Wendland, Piecewise polynomial, positive definite and compactly supported radial functions of minimal degree, Advances in Computational Mathematics 4 (1) (1995) 389–396.
[104] W. Rudin, Real and complex analysis, Tata McGraw-Hill, 2006.
[105] J.M. Melenk, I. Babuka, The partition of unity finite element method: basic theory and applications, Computer Methods in Applied Mechanics and Engineering 139 (1–4) (1996) 289–314.
[106] F. Losasso, F. Gibou, R. Fedkiw, Simulating water and smoke with an octree data structure, ACM Transactions on Graphics 23 (3) (2004) 457–462.
[107] D. Cohen-Steiner, P. Alliez, M. Desbrun, Variational shape approximation, ACM Transactions on Graphics 23 (August 2004) 905–914.
[108] V. Arsigny, P. Fillard, X. Pennec, N. Ayache, Fast and simple calculus on tensors in the Log-Euclidean framework, Medical Image Computing and Computer-Assisted Intervention, 2005, pp. 115–122.
[109] W. Liu, E. Ribeiro, A novel consistency regularizer for meshless nonrigid image registration, Advances in Visual Computing, Springer, 2010, pp. 242–251.
[110] W. Liu, E. Ribeiro, A meshless method for variational nonrigid 2-d shape registration, Advances in Visual Computing, Springer, 2010, pp. 262–272.
[111] P. Lancaster, K. Salkauskas, Surfaces generated by moving least squares methods, Mathematics of Computation 37 (155) (1981) 141–158.
[112] S. Fleishman, D. Cohen-Or, C.T. Silva, Robust moving least-squares fitting with sharp features, ACM Transactions on Graphics 24 (July 2005) 544–552.
[113] T. Chen, S. Kim, J. Zhou, D. Metaxas, G. Rajagopal, N. Yue, 3D Meshless Prostate Segmentation and Registration in Image Guided Radiotherapy, Medical Image Computing and Computer-Assisted Intervention, 2009, pp. 43–50.
[114] T. Chen, S. Kim, S. Goyal, S. Jabbour, J. Zhou, G. Rajagopal, B. Haffty, N. Yue, Object-constrained meshless deformable algorithm for high speed 3D nonrigid registration between CT and CBCT, Medical Physics 37 (1) (2010) 197–210.
[115] M. Wand, B. Adams, M. Ovsjanikov, A. Berner, M. Bokeloh, P. Jenke, L. Guibas, H.P. Seidel, A. Schilling, Efficient reconstruction of nonrigid shape and motion from real-time 3D scanner data, ACM Transactions on Graphics 28 (2) (2009) 1–15.
[116] M. Fleute, S. Lavallée, Nonrigid 3-d/2-d registration of images using statistical models, Medical Image Computing and Computer-Assisted Intervention, 1999, pp. 138–147.
[117] D. Cremers, C. Schnórr, Statistical shape knowledge in variational motion segmentation, Image and Vision Computing 21 (1) (2003) 77–86.
[118] T. Petrila, D. Trif, Basics of fluid mechanics and introduction to computational fluid dynamics, Springer Verlag, 2005.
[119] F. Irgens, Continuum mechanics, Springer Verlag, 2008.
[120] Jing Yuan, Schörr Christoph, Steidl Gabriele, Simultaneous higherorder optical flow estimation and decomposition, SIAM Journal of Scientific Computing 29 (6) (2007) 2283–2304.
[121] E. D'Agostino, F. Maes, D. Vandermeulen, P. Suetens, A viscous fluid model for multimodal non-rigid image registration using mutual information, Medical Image Computing and Computer-Assisted Intervention, 2002, pp. 541–548.
[122] Y. Chen, H.D. Tagare, S. Thiruvenkadam, F. Huang, D. Wilson, K.S. Gopinath, R.W. Briggs, E.A. Geiser, Using prior shapes in geometric active contours in a

variational framework, International Journal of Computer Vision 50 (3) (2002) 315–328.
[123] F. Li, L. Xu, P. Guyenne, J. Yu, Recovering fluid-type motions using Navier-Stokes potential flow, IEEE Conference on Computer Vision and Pattern Recognition, 2010, pp. 2448–2455.
[124] R. Bajcsy, S. Kovačič, Multiresolution elastic matching, Computer Vision, Graphics, and Image Processing 46 (1) (1989) 1–21.
[125] D. Terzopoulos, J. Platt, A. Barr, K. Fleischer, Elastically deformable models, Proceedings of the 14th Annual Conference on Computer Graphics and Interactive Techniques, 1987, pp. 205–214.
[126] T. McInerney, D. Terzopoulos, Deformable models in medical image analysis, Proceedings of the Workshop on Mathematical Methods in Biomedical Image Analysis, 1996, pp. 171–180.
[127] D.N. Metaxas, Physics-based deformable models: applications to computer vision, graphics, and medical imaging, Kluwer Academic Publishers, 1997.
[128] C. Broit. Optimal registration of deformed images. PhD thesis, University of Pennsylvania, Philadelphia, PA, USA, 1981.
[129] E. Haber, J. Modersitzki, A multilevel method for image registration, SIAM Journal on Scientific Computing 27 (5) (2006) 1594–1607.
[130] P. Shi, A.J. Sinusas, R.T. Constable, J.S. Duncan, Volumetric deformation analysis using mechanics-based data fusion: Applications in cardiac motion recovery, International Journal of Computer Vision 35 (1) (1999) 87–107.
[131] A. Hagemann, K. Rohr, H.S. Stiehl, U. Spetzger, J.M. Gilsbach, Biomechanical modeling of the human head for physically based, nonrigid image registration, IEEE Transactions on Medical Imaging 18 (10) (1999) 875–884.
[132] C. Davatzikos, Spatial transformation and registration of brain images using elastically deformable models, Computer Vision and Image Understanding 66 (2) (1997) 207–222.
[133] A. Cuzol, E. Memin, A stochastic filtering technique for fluid flow velocity fields tracking, IEEE Transaction on Pattern Analysis and Machine Intelligence 31 (7) (July 2009) 1278–1293.
[134] N. Papadakis, E. Mémin, Variational assimilation of fluid motion from image sequence, SIAM Journal of Image Sciences 1 (4) (2008) 343–363.
[135] P. Ruhnau, C. Schnórr, Optical stokes flow estimation: an imagingbased control approach, Experiments in Fluids 42 (1) (2007) 61–78.
[136] L. Amodei, M.N. Benbourhim, A vector spline approximation, Journal of Approximation Theory 67 (1) (1991) 51–79.
[137] C.O.S. Sorzano, P. Thevenaz, M. Unser, Elastic registration of biological images using vector-spline regularization, IEEE Transactions on Biomedical Engineering 52 (4) (2005) 652–663.
[138] I. Arganda-Carreras, C. Sorzano, R. Marabini, J. Carazo, C. Ortiz-de Solorzano, J. Kybic, Consistent and elastic registration of histological sections using vector-spline regularization, ECCV Workshop: Computer Vision Approaches to Medical Image Analysis, 2006, pp. 85–95.
[139] G.P. Penney, J. Weese, J.A. Little, P. Desmedt, D.L.G. Hill, A comparison of similarity measures for use in 2-D-3-D medical image registration, IEEE Transactions on Medical Imaging 17 (4) (2002) 586–595.
[140] T. Vercauteren, X. Pennec, A. Perchant, N. Ayache, Symmetric log-domain diffeomorphic registration: A demons-based approach, Medical Image Computing and Computer-Assisted Intervention, 2008, pp. 754–761.
[141] A. Klein, J. Andersson, B.A. Ardekani, J. Ashburner, B. Avants, M.C. Chiang, G.E. Christensen, D.L. Collins, J. Gee, P. Hellier, J.H. Song, M. Jenkinson, C. Lepage, D. Rueckert, P. Thompson, T. Vercauteren, R.P. Woods, J.J. Mann, R.V. Parsey, Evaluation of 14 nonlinear deformation algorithms applied to human brain MRI registration, Neuroimage 46 (3) (2009) 786–802.
[142] G. Christensen, X. Geng, J. Kuhl, J. Bruss, T. Grabowski, I. Pirwani, M. Vannier, J. Allen, H. Damasio, Introduction to the non-rigid image registration evaluation project (NIREP), Third International Workshop on Biomedical Image Registration, 2006, pp. 128–135.
[143] S.S. Klein, A. andd Ghosh, B. Avants, B.T. Yeo, B. Fischl, B. Ardekani, J.C. Gee, J.J. Mann, R.V. Parsey, Evaluation of volume-based and surface-based brain image registration methods, NeuroImage 51 (1) (2010) 214–220.
[144] C.A. Cocosco, V. Kollokian, K.S.K. Remi, G.B. Pike, A.C. Evans, Brainweb: Online interface to a 3D MRI simulated brain database, International Conference on Functional Mapping of the Human Brain, 1997.
[145] K. Okamoto, S. Nishio, T. Kobayashi, T. Saga, K. Takehara, Evaluation of the 3D-PIV standard images (PIV-STD project), Journal of Visualization 3 (2) (2000) 115–123.
[146] D. Rueckert, A. Frangi, J. Schnabel, Automatic construction of 3D statistical deformation models using non-rigid registration, Medical Image Computing and Computer-Assisted Intervention, 2001, pp. 77–84.
[147] T. Vercauteren, X. Pennec, A. Perchant, N. Ayache, Diffeomorphic demons: Efficient non-parametric image registration, NeuroImage 45 (1) (2009) 61–72.
[148] A. Andreopoulos, J.K. Tsotsos, Efficient and generalizable statistical models of shape and appearance for analysis of cardiac MRI, Medical Image Analysis 12 (3) (2008) 335–357.
[149] M.J. Ackerman, The visible human project, Proceedings of the IEEE 86 (3) (2002) 504–511.
[150] T. Yoo, M. Ackerman, M. Vannier, Toward a common validation methodology for segmentation and registration algorithms, Medical Image Computing and Computer-Assisted Intervention, 2000, pp. 217–225.
[151] M. Sermesant, C. Forest, X. Pennec, H. Delingette, N. Ayache, Deformable biomechanical models: Application to 4D cardiac image analysis, Medical Image Analysis 7 (4) (2003) 475–488.
[152] R.M. Koch, M.H. Gross, F.R. Carls, D.F. von Búren, G. Fankhauser, Y.I.H. Parish, Simulating facial surgery using finite element models, Proceedings of the 23rd Annual Conference on Computer Graphics and Interactive Techniques, ACM, 1996, pp. 421–428.
[153] D.W. Shattuck, M. Mirza, V. Adisetiyo, C. Hojatkashani, G. Salamon, K.L. Narr, R.A. Poldrack, R.M. Bilder, A.W. Toga, Construction of a 3D probabilistic atlas of human cortical structures, NeuroImage 39 (3) (2008) 1064–1080.
[154] P. Ruhnau, A. Stahl, C. Schnórr, Variational estimation of experimental fluid flows with physics-based spatio-temporal regularization, Measurement Science and Technology 18 (3) (2007) 755–763.
[155] M. Pantic, M. Valstar, R. Rademaker, L. Maat, Web-based database for facial expression analysis, IEEE International Conference on Multimedia and Expo, 2005, pp. 5–9.
[156] S. Koelstra, M. Pantic, Non-rigid registration using free-form deformations for recognition of facial actions and their temporal dynamics, IEEE International Conference on Automatic Face and Gesture Recognition, 2008, pp. 1–8.
[157] L. Yin, X. Chen, Y. Sun, T. Worm, M. Reale, A high-resolution 3D dynamic facial expression database, IEEE International Conference on Automatic Face and Gesture Recognition, 2009, pp. 1–6.
[158] Y. Sun, X. Chen, M. Rosato, L. Yin, Tracking vertex flow and model adaptation for three-dimensional spatiotemporal face analysis, IEEE Transactions on Systems, Man and Cybernetics, Part A: Systems and Humans 40 (3) (2010) 461–474.
[159] J. Ashburner, A fast diffeomorphic image registration algorithm, Neuroimage 38 (1) (2007) 95–113.
[160] X. Huang, N. Paragios, D.N. Metaxas, Shape registration in implicit spaces using information theory and free form deformations, IEEE Transactions on Pattern Analysis and Machine Intelligence 28 (8) (2006) 1303–1318.
[161] U. Grenander, I. Michael, M.I. Miller, Computational anatomy: an emerging discipline, Quarterly of Applied Mathematics LVI (4) (1998) 617–694.
[162] D. Rueckert, P. Aljabar, R. Heckemann, J. Hajnal, A. Hammers, Diffeomorphic registration using B-splines, Medical Image Computing and Computer-Assisted Intervention, 2006, pp. 702–709.
[163] S. Periaswamy, H. Farid, Medical image registration with partial data, Medical Image Analysis 10 (3) (2006) 452–464.
[164] B. Li, A.A. Young, B.R. Cowan, GPU accelerated non-rigid registration for the evaluation of cardiac function, Medical Image Computing and Computer-Assisted Intervention, 2008, pp. 880–887.
[165] X. Gu, H. Pan, Y. Liang, R. Castillo, D. Yang, D. Choi, E. Castillo, A. Majumdar, T. Guerrero, S.B. Jiang, Implementation and evaluation of various demons deformable image registration algorithms on a GPU, Physics in Medicine and Biology 55 (1) (2010) 207–219.
[166] R. Shams, P. Sadeghi, R. Kennedy, R. Hartley, A survey of medical image registration on multi-core and GPU, IEEE Signal Processing Magazine 27 (2) (2010) 50–60.
[167] T. Schiwietz, R. Westermann, GPU-PIV, Proceedings of the Vision, Modeling, and Visualization Conference, 2004, pp. 151–158.
[168] M. Prastawa, E. Bullitt, G. Gerig, Synthetic ground truth for validation of brain tumor MRI segmentation, Medical Image Computing and Computer-Assisted Intervention, 2005, pp. 26–33.
[169] W. Van Hecke, J. Sijbers, S. De Backer, D. Poot, P.M. Parizel, A. Leemans, On the construction of a ground truth framework for evaluating voxel-based diffusion tensor MRI analysis methods, NeuroImage 46 (3) (2009) 692–707.
[170] P. Hellier, C. Barillot, I. Corouge, B. Gibaud, G. Le Goualher, D.L. Collins, A. Evans, G. Malandain, N. Ayache, G.E. Christensen, et al., Retrospective evaluation of intersubject brain registration, IEEE Transactions on Medical Imaging 22 (9) (2003) 1120–1130.